UNIVERSIDADE D
COIMBRA

Asif Guliyev

INFLUENCE OF VOLTAGE OSCILLATION PULSE-OFF TIME IN A DOMS ON THE PROPERTIES OF HARD HYDROGEN-FREE DLC COATINGS FOR THE AUTOMOTIVE INDUSTRY

VOLUME 1

Dissertação no âmbito do Mestrado Conjunto Europeu em Tribologia de Superfícies e Interfaces orientada pelo Doutor João Carlos Barbas de Oliveira e Doutor Fábio Emanuel de Sousa Ferreira apresentada ao Departamento de Engenharia Mecânica da Faculdade de Ciências e Tecnologia da Universidade de Coimbra

Julho de 2019

Acknowledgements

Completion of Joint European Master's Degree without collaboration with different people and institutes wasn't possible for me alone. First of all, I want to thank Doctor Joao Carlos Oliveira for his kindness and helpful character. Dr. Carlos provided a chance for me to work in an academic environment and advised me through my Master thesis project. During my research, whenever I encountered a problem he helped me with his broad knowledge background and experience.

I need to specially thank Fabio Ferreira, Ricardo Serra, and Manuel Evaristo for their support and helps during this 6 month of working with them. They provided help whenever I want any support and they show their ultimate kindness to me.

TRIBOS consortium gave me the chance to do an amazing master's degree abroad and add to my experiences during last two years. Hereby, I want to thank Professor Mitjan Kalin, Professor Ardian Morina, Professor Nazanin Emami and Professor Bruno Trindade for selecting me as a TRIBOS student.

Thank you all

Abstract

Recent developments such as turbocharging and downsizing in the automotive industry to enhance engine efficiency and reduce emissions are giving rise to the higher operation temperatures and loading densities in the internal combustion engines. Increased temperature stability (up to 500 °C) will be required for coatings of future's engines compared to ones of present day. Hard tetrahedral DLC coatings (ta-C coatings) are very attractive to be used for automotive industry as they exhibit very low coefficient of friction and perform very well under mixed and boundary lubrication.

This research project was carried out in the framework of the European TANDEM project which aims at developing a new generation of ta-C coatings. It is a follow up of the work previously carried out at CEMMPRE where substrate bias was optimized (-80 V) at 124 µs of oscillation pulse-off time. In this work, DLC coatings were deposited by deep oscillations magnetron sputtering (DOMS), a variant of high power magnetron sputtering (HiPIMS). The main objective is to study influence of oscillation pulse-off time (t_{off}) in two series of depositions (at 0.4 Pa and 0.8 Pa) on the structural, mechanical, and tribological properties of the DLC films deposited by DOMS with substrate biasing. SEM, AFM, XPS analysis (only for 2 films), hardness, stress, and pin-on-disc measurements were carried out for studying DLC films.

Regarding the DLC films deposited at 0.4 Pa, the hardness of the films shows significant changes with t_{off}, most likely due to corresponding changes in the sp^3/sp^2 fraction of the films. However, the specific wear rate of the films remains very similar excepting for the film deposited at the highest t_{off} (124 µs) which has a slightly denser microstructure. Overall, it can be concluded that decreasing t_{off} does result in improved tribological properties, but better mechanical properties (i.e hardness) can be obtained. At a deposition pressure of 0.8 Pa, decreasing t_{off} from 124 to 84 or even 64 µs results in both a lower friction coefficient and significantly lower wear rates without any appreciable loss of hardness. In fact, the specific wear rate of the film deposited at t_{off} = 84 µs is not only the lowest specific wear rate measures in this work but it is also significantly lower than the specific wear rates measures in previous works about the deposition of DLC films by DOMS.

Keywords: HiPIMS, DOMS, Sputtering, Carbon, Tribology, Friction coefficient, Wear rate

Table of Contents

List of Figures

List of Tables

Chapter 1: Introduction

Recent developments such as turbo-charging, start-stop engines, downsizing and low viscosity lubricants have become popular in the automotive industry to enhance engine efficiency. Operating temperatures and loading densities on components are getting increasingly higher because of these developments that lead to various industrial challenges which are presented below:

- High friction and wear can cause more breakdowns and failures. Therefore, the vehicle performance may be reduced and engine breakdowns appear.
- To overcome excess friction, consumption of energy gets higher which results in increasing costs for machine operation.

It has been found that friction is one of the efficiency losses in internal combustion engines (ICE). Challenges of decreasing fuel consumption and emission have always been faced in designing engines since every component has its share in the frictional mechanical loss. A significant share of frictional loss comes from piston rings, so frictional losses can be reduced noticeable by optimizing the interaction between piston rings and cylinder [1]. Energy consumption shares of a gasoline engine are presented in Figure 1. It shows that the piston rings are responsible for 24 % of the total frictional losses in the gasoline engine.

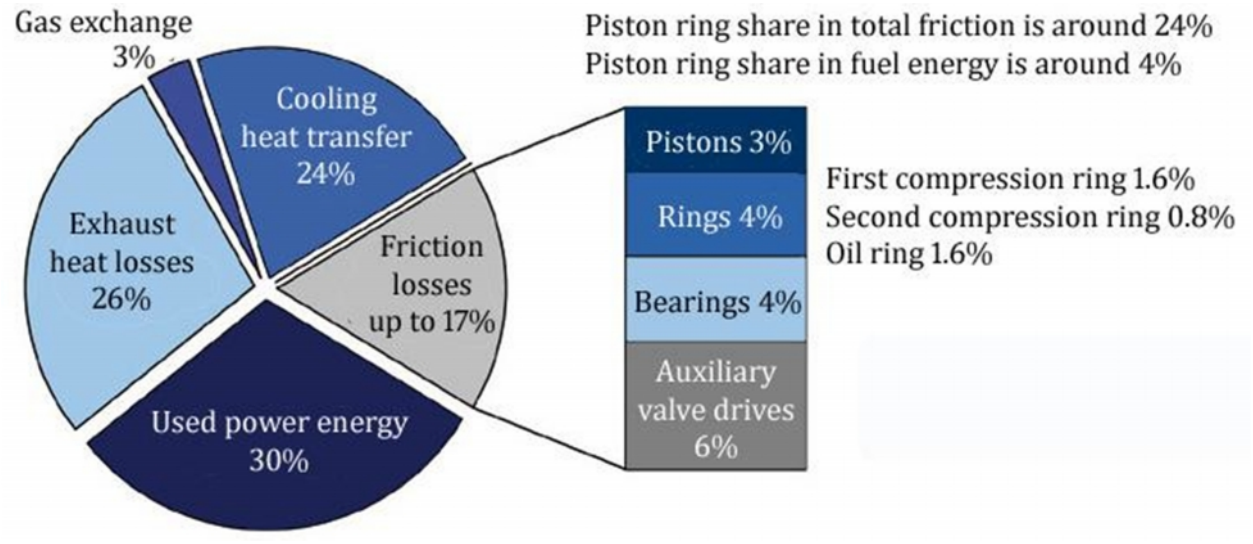

Figure 1: Energy distribution diagram of gasoline engine [1].

To reduce mechanical losses and to enhance fuel efficiency, scientists are studying materials/coatings which could have low friction and wear in the piston ring-cylinder contacts. Notable attempts have been taken in the way of developing new energy-conserving lubricants, friction modifiers, anti-wear additives, surface texturing and hard ceramic coatings [2,3]. Hard ceramic coatings are the most recent coatings for piston rings. These coatings can be deposited by chemical vapor deposition or physical vapor deposition which can be titanium nitride (TiN) and chromium nitride (CrN) coatings. Compared to titanium nitride coatings, chromium nitride coatings are less hard, but they have a higher resistance to oxidation and stresses. It has been shown in the work of Lin et al. [4] that chromium nitride coatings can support the performance of piston rings under harsh conditions as the thickness of coatings is increased. On the other hand, the dry friction coefficient of these coatings is higher that doesn't contribute significantly to the reducing of fuel consumption. TiSiCN nanocomposite coatings exhibit reduced frictional losses and wear in the piston rings of internal combustion engines which have also better tribological properties and high hardness [5].

There are also many other coatings which provide good tribological properties and hardness. Diamond-like carbon (DLC) coatings are considered as one of the best coatings for the automotive industry according to their extremely smooth surfaces and very low coefficient of friction [6]. Furthermore, DLC coatings have extremely good resistance towards adhesive and abrasive wear which makes them appropriate to be used in mechanical applications where very high contact pressures are experienced [7]. However, a real challenge in evaluating these coatings for their suitability in automotive applications is to see how these coatings respond to the recent developments i.e. turbocharging and downsizing in the automotive industry. These developments are giving rise to the need for increasingly high operating temperatures and loading densities on the components [8].

The conventional DLC films have excellent tribological properties, but they lose performance at elevated temperatures such as 300 °C. In the interface of ring and cylinder, temperatures can even exceed 400 °C. According to this forthcoming increase in temperature, novel diamond-like carbon coatings such as hydrogen free hard tetrahedral DLC (ta-C) coatings are needed which are stable at high temperatures. These coatings took great attraction to be used in the automotive industry as they have excellent performance at mixed and boundary lubrication

regimes. However, a great amount of generated internal stresses have been the main limitation for these coatings since delamination can occur when internal stresses exceed a critical value [9]. Eventually, developing new DLC coatings has been the topic of researches that can perform well in high temperatures and other harsh environments without any delamination of the films.

Deposition of ta-C coatings can be conducted by highly ionized physical vapor deposition (PVD), such as cathodic arc deposition since the bombardment of ions with hyper-thermal energy during the deposition has great impact on sp^3 content. The main disadvantage of this technique is macro particle ejection from the target which results with the degradation of mechanical properties and surface roughness increase. Filtering plasma can help to solve this issue, but it is an expensive technique also also significantly reduces the deposition rate. Another PVD technique which is called direct current magnetron sputtering (DCMS) can be used to deposit DLCs with a smooth surface. As being atomic deposition, this technique allows controlling the surface roughness. However, the present state of the art DLCs deposited by conventional magnetron sputtering have low sp^3 content (up to 45%) and, therefore, much lower film density (1.8–2.3 g/cm3) and hardness (<20 GPa) than DLCs deposited by cathodic arc deposition

There is a new technique which is called High Power Impulse Magnetron Sputtering (HiPIMS) used for depositing hard DLCs. In this technique, the ionization of a high fraction of sputtered atoms takes place due to 2–3 orders of magnitude higher plasma densities than DCMS. However, the conventional argon based HiPIMS process allows a very low fraction of carbon to be ionized because of the low carbon ionization cross-section by electron impact. When partially or totally replacing standard sputtering gas Ar with Ne, additional carbon ions can be produced in HiPIMS. Recent studies show that using very short high voltage pulses can lead to an increased sp^3/sp^2 ratio in DLC coatings. Deep Oscillations Magnetron Sputtering (DOMS) which is a variant of HiPIMS was used in this work for depositing DLC films. As DOMS pulse contains a packet of short high voltage single oscillations, it is very suitable for depositing DLC films with high sp^3 content.

The main purpose of this thesis is to study DLC films deposited by using DOMS in order to gain high hardness, good tribological properties and higher stability at high temperature for application in piston rings. In the previous research which was done at CEMMPRE, the effect of both substrate bias voltage and the addition of Ne as a discharge gas on structural and

mechanical properties of hard hydrogen free DLC coatings were studied. Overall, substrate biasing increase resulted in smoother and denser DLC films. Mass density and hardness of coatings increased from 1.8 to 2.5 g/cm^3 and from 15 to 23 GPa, respectively. On the other hand, smoother and denser films were experienced when increasing Ne content and maximum hardness of 24 GPa was achieved. It was found that a substrate bias of – 80 V was the best compromise in order to obtain hard dense DLC films without giving rise to residual stress build up and subsequent delamination of the DLC films. Although the substrate bias is the most influent deposition parameter in the deposition of DLC films by magnetron sputtering based processes, fine tune of the DLC mechanical and tribological properties can be carried out by optimizing other deposition parameters such as the deposition pressure. In DOMS, the time variation of the voltage pulses is also an important experimental factor. Parameters such as the period and duration of the short high voltage oscillations applied to the cathode during the depositions can significantly impact the films properties. Decreasing the time between the voltage oscillations (t_{off}) influence the films properties as lower values of t_{off} as more ionic species are present in the plasma at the beginning of each oscillation. On the other hand, decreasing t_{off} also results in localized arcing on the carbon target surface which can be beneficial for the deposition of DLC films with higher sp^3/sp^2 ratios. The main objective of this work was to study the influence of variation of voltage oscillation pulse-off time (t_{off}) on the structural, mechanical and tribological properties of the DLC films deposited by DOMS with substrate biasing at – 80 V. The substrate biasing used in this work was already defined by previous research work.

This research project is a master thesis project in European Joint Masters in Tribology of Surfaces and Interfaces. This work is part of both the European TANDEM and the national HardRings projects which aim to develop a new generation of significantly improved hard hydrogen-free DLC (ta-C) coatings, based on HiPIMS, for piston rings in internal combustion engines. In this research, State of the art, Experimental conditions for DLC deposition and Characterization techniques, Results, and Discussion and at the end Conclusion are presented.

Chapter 2: State of the art

2.1 Piston Ring

The piston rings are one of the essential parts of the internal combustion engines. Piston rings are deployed in internal combustion engines to reduce oil consumption and power loss. For diminishing friction, wear and heat loss, there is usually a gap between piston and cylinder. Two or three piston rings are placed on the piston to insulate between the compression part and vacuum part. These three piston rings are:

- Compression/ pressure rings: Usually, they are installed on the top of the piston for sealing gasses in the combustion chamber and help in the dissipation of generated heat in the engine and cool it down.
- Intermediate/ scraper rings: They are positioned after the compression ring and the function of them is wiping off the oil and lubricants on the piston wall.
- Oil control rings: The function of these rings is controlling the amount of lubricant stuck on the wall for the purpose of lubrication and economic efficiency.

Since there is a direct contact between the piston rings and the cylinder liner, wear and deterioration of piston can be experienced which affects engine performance negatively and increase fuel consumption. Hard coatings such as thermal barrier coatings (ZrO_2, Al_2O_3 and Al_2O_3-TiO_2), DLCs, composite coatings, and ceramic coatings can be used for eliminating these issues [10].

2.2 DLC coatings

Carbon is one of the unique elements in the periodic table with the highest number of allotropes. Carbon-based coatings, such as DLCs, Carbon-Nitride, Boron Carbide have been developed to be used in a high number of applications due to excellent tribological properties in various operating conditions [11]. Diamond-like carbon is a general expression used for a lot of carbon films such as amorphous carbon films (a-C), hydrogenated amorphous carbon (a-C:H) and tetrahedral amorphous carbon (ta-C).

In general, it is a mixture of various bonding components such as C-C sp^3, C-C sp^2, C-H sp^1 bonds where diamond-like behavior comes from C-C sp^3 bonds which have the main effect on the mechanical and tribological properties of DLC. Mechanical properties such as Young's

modulus and density are linearly proportional to the sp^3 fraction and the main reason of the presence of carbon-based coatings in various engineering applications is their outstanding mechanical and tribological properties [12]. These carbon-based films help in controlling the friction and wear in engineering components. The combination of these unique properties of DLC films makes them attractive for several applications in the industries of oil-gas, automotive, medical, military and aerospace.

Amorphous carbon in thin films can be grown in different forms including hydrogen-free form and hydrogenated amorphous carbon and with a wide range of properties due to various bonding components (sp^1, sp^2, and sp^3, Figure 2). When the sp^3 content is noticeable high (90%), it is called the ta-C film [13]. Each of the carbon contains four valence electrons that can make four distinct bonds. In the case of sp^1 hybridization state, two valence electrons out of available four establish σ (sigma) bonds which are directed along a plane with its adjacent atoms, usually they are carbon atoms. The rest of valence electrons form a π (pi) bond in y and z planes. In the three-fold coordinated sp^2 configuration like in graphite, three valence electrons are assigned to trigonally directed sp^2 orbitals that make σ bonds in a plane. The last valence electron of sp^2 lies in a π orbital, which lies normal to the σ bonding plane. This π orbital makes a weaker π bond with a π orbital on one or more adjacent atoms [14]. In the case of sp^3 configuration like in diamond, all four valence electrons of carbon are allocated to a tetrahedrally directed sp^3 orbital that forms a strong bond with the neighboring atom.

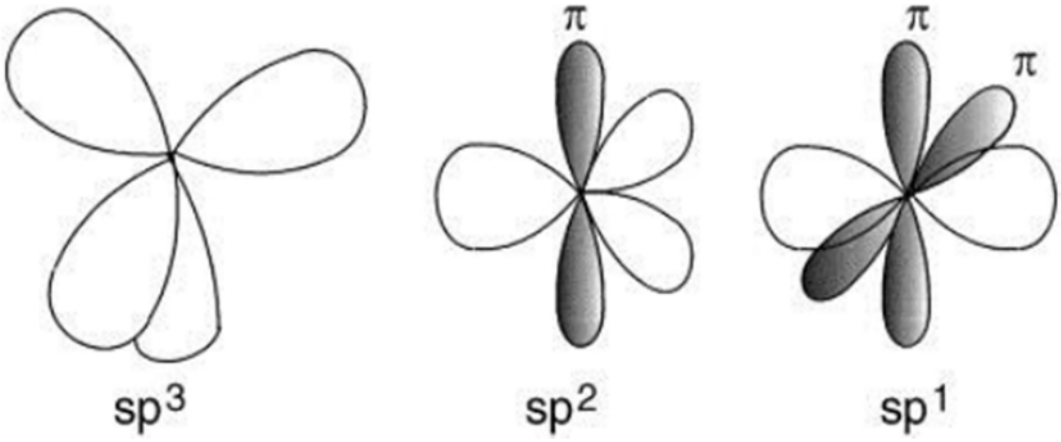

Figure 2: sp^3, sp^2 and sp^1 hybridization states [15].

The ternary phase diagram of amorphous carbon with different sp^2, sp^3, and sp^1 content is presented in Figure 3. As can be seen from the diagram, graphitic and glassy carbon are placed in

the bottom left-hand corner with the largest sp^2 fraction and free of hydrogen. Ta-C films are formed by increasing sp^3 fraction. When hydrocarbons are used as precursors, hydrogen presence is unavoidable. This hydrogen leads two regions in the middle of the diagram, tetrahedral hydrogenated carbon (ta-C:H) and hydrogenated amorphous carbon (a-C:H). Increasing hydrogen content leads to the formation of polymers. Eventually, if hydrogen content is higher than carbon which is depicted at the bottom righ-hand corner, no films are formed [16].

In Figure 3, there is a decrease in the density of sp^2 bonding from the left to the right. As sigma bonds are stronger than π bonds, the ta-C films which are richer in sp^3 (like Diamond) show higher hardness than the other carbon hybridization states.

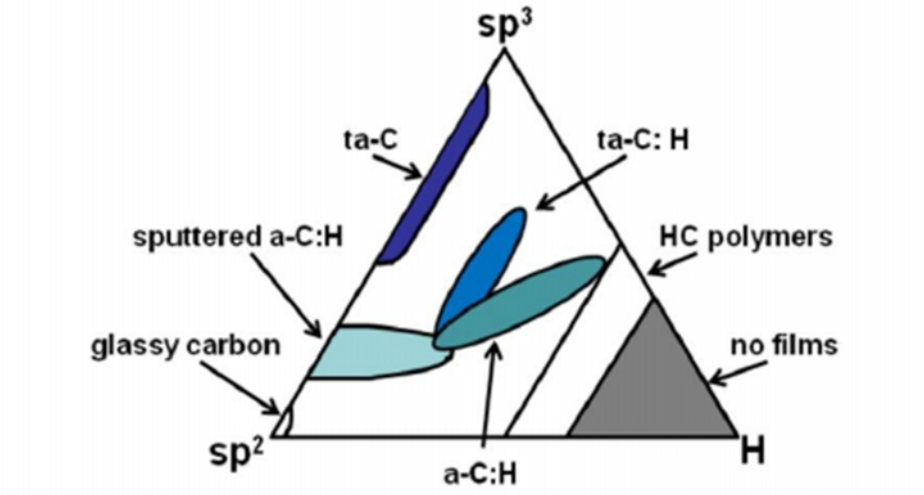

Figure 3: Phase diagram for amorphous carbon [16].

Recently, scientists developed non-usual DLC films with nano-phases and structures. By having less than a few micrometers thickness, these coatings are considered as very thin. Exact evaluation of the mechanical properties of these thin coatings is very difficult. New advancements in mechanical testing instruments make these measurements much easier. DLC coatings show a variety of mechanical properties with hardness ranging from a few GPa to over 60 GPa. Furthermore, recent developments in the coating deposition techniques help scientists to control the properties of DLC films [17].

It has been studied that residual stresses are generated when depositing thin films. The coating is peeled off when residual stresses are higher than the set threshold value of stress due to high-stress gradient between the coating and substrate [15]. Various elements such as Ti, Cr,

Co, Al and Si which are shown Figure 4 can be added to the DLC coatings (doped or alloyed DLC) to decrease these residual stresses. Alloying elements influence altering properties of the coating such as thermal stability, electrical resistivity, and surface energy. In addition, when metals are used as substrates, DLC coatings may experience adhesion issues because of diffusion of carbon into the steel and growth of coating is retarded. Furthermore, as coefficients of thermal expansion of coatings and steels are not compatible, a large amount of internal stresses and poor adhesion is achieved [18]. To overcome these issues, some interlayers and surface modification techniques have been developed.

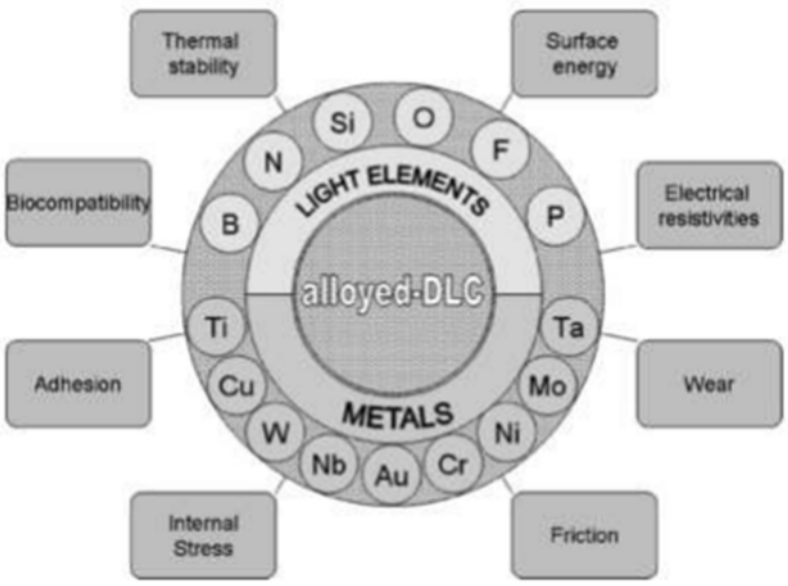

Figure 4: Scheme of known DLC dopants to improve particular properties [19].

Some studies indicate that conventional DLC coatings have not been performed well at elevated temperatures. To overcome this issue, new coatings types such as hard hydrogen free DLCs were made as hydrogen has a great effect on properties of DLC films. Increasing hydrogen content results in decreased Young's modulus and hardness. According to a high fraction of sp^3 hybridization, hydrogen free DLC coatings have excellent properties (i.e. harder than steels) and good thermal stability. Moreover, they also exhibit high toughness and good tribological properties and a few of recently developed DLCs have excellent resistance against wear under sliding conditions.

2.3 Deposition techniques for DLC coatings

The deposition of DLC coatings can be carried out by several techniques which are shown in Figure 5 such as cathodic arc evaporation (CAE), pulsed laser deposition, ion beam deposition, plasma immersion ion deposition, plasma enhanced chemical vapor deposition and magnetron sputtering, but some of these methods are not suitable for industrial purposes [20]. Ion bombardment during these deposition processes has a significant influence on the structure and properties of DLC films and the proportion of sp^3 bonding particularly depends on the energy level of ion bombardment. To attain a great amount of sp^3 bonding, there should be properly controlled ion energies. A commonly used technique for depositing DLC films with a great amount of sp^3 bonding is CAE. The sp^3 fraction of DLC films deposited by this technique is in the range of 70-90% [21].

A high proportion of sp^3 bonding results in high residual stresses on the films and high hardness [22]. Therefore, DLC films deposited by CAE generally show high hardness. It has been reported in the literature that hardness values are in the range of 15-30 GPa and some studies show that it is even above 50 GPa [23]. However, deposited films by CAE usually have the incorporation of macro-particles during the arc process [24]. In order to remove atomic clusters from the beam before deposition, filtered cathodic arc vacuum can be used, but some of the magnetic filtering designs do not work well with high melting point graphite. At the same time, the rate of deposition decreases dramatically [25]. The other challenge is brittleness of ta-C films which weaken the adhesion in films and decrease the thickness of the films [26].

One of the other methods for depositing DLC films which are suitable for laboratory studies is mass-selected ion beam deposition. Since single ion species can be selected, this technique allows higher control. On the other hand, the deposition rate by this method is lower and equipment is expensive.

Magnetron sputtering is another broadly used technique for depositing ta-C films. Due to low ionization degrees (ion/neutral ratio), DLC films with low sp^3 bonding fractions and less dense microstructure are obtained. This usually happened when DC and RF are used as power sources during magnetron sputtering. The hardness of films deposited by magnetron sputtering is in the range of 5-20 GPa.

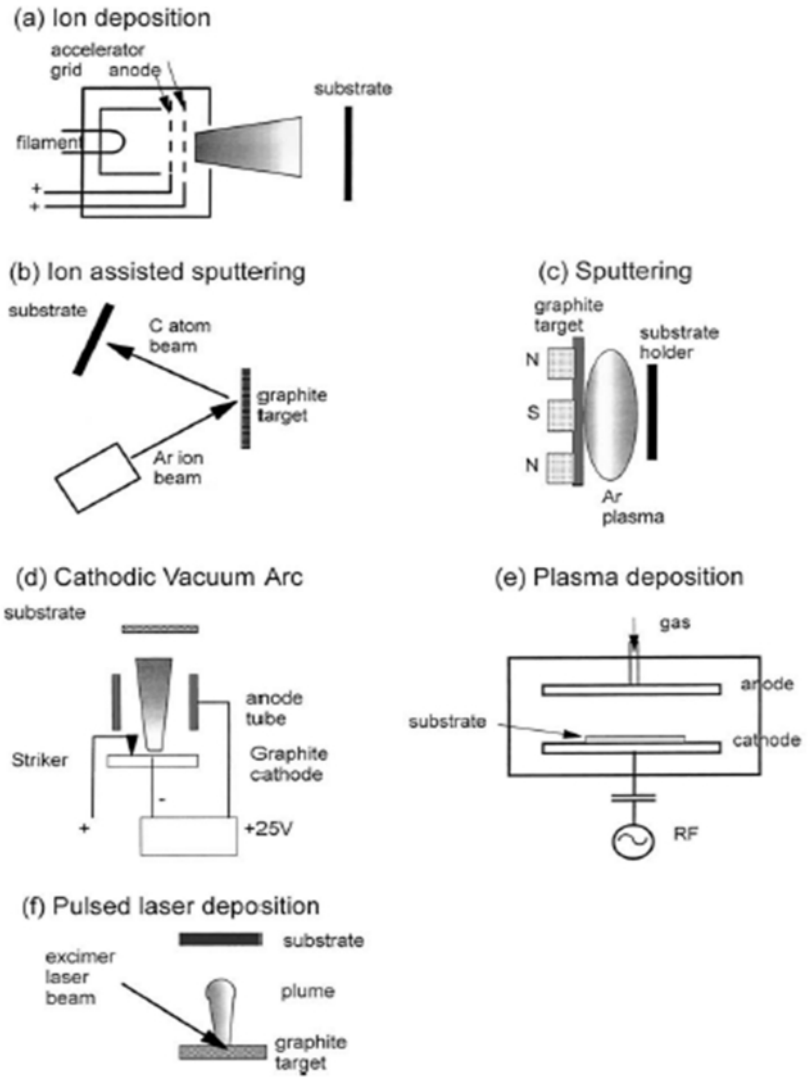

Figure 5: Various techniques used for depositing DLC films [15].

According to Robertson's carbon growth model, the largest sp^3 fraction can be obtained at an ion energy of 100 eV [27]. Ion energy can be controlled by adjusting the negative substrate bias voltage. Traditional DC and RF magnetron sputtering have challenges in increasing the ionization degree of carbon and gas species due to low electron density in the plasma.

It has been shown in recent studies that many metal target species can be notably ionized by high pulsed power on the target [28]. This is carried out by a technique which is known as high power impulse magnetron sputtering (HiPIMS). According to 2-3 orders of magnitude higher plasma densities than in DCMS, a high proportion of sputtered atoms is ionized. Argon is

used in the standard HiPIMS process where an ionized fraction of C is very low because of the low carbon cross-section by electron impact. Partially reducing gas pressure inside the chamber allows further C ions to be produced. Recent literature shows that using very short high voltage pulses cause a significant increase in the sp^3/sp^2 fraction in the DLC films and denser microstructure.

According to Sarakinos et al. [29], single-pulse HiPIMS can be used to deposit amorphous carbon films with bond fraction up to 45% and density up to 2.2 g/cm^3 that is greater than the ones done by DCMS. Furthermore, another suggestion came from Aijaz et al. [30] regarding using Ne as sputtering gas and increasing carbon ionization in a single-pulse HiPIMS discharge. However, tribological and mechanical properties of obtained carbon films are limited. Recent literature shows that only a few studies have been carried out about depositions of DLC coatings by HiPIMS utilizing oscillatory voltage pulses. The main parameters which can have an impact on the flux and energy of ions are the negative substrate bias voltage (Vb), the working pressure (P), and the peak target current density (J) that are essential for determining the structure and properties of the films. In this work, the deposition of DLC films was carried out by HiPIMS-DOMS.

2.4 HiPIMS

Sputtering is a physical phenomenon where the ejection of target atoms occurs by incident ions. The incident ions are extracted from plasma in magnetron sputtering. By negative applied voltage, ions generated in plasma are directed onto the target and eventually, atoms from the target are sputtered due to various interactions. Using magnetron close to the target where the magnetic field is generated increase the collision probability of electrons with neutral gas atoms, so sputtering efficiency is increased [31].

Kouznetsov et al. [32] firstly introduced HiPIMS which is a technique used for improving conventional magnetron sputtering by the addition of pulsed power technology. HiPIMS is a pulsed magnetron sputtering and in this technique, peak power exceeds time-averaged power by two orders of magnitude [33].

The major feature of HiPIMS is the combination of sputtering from standard magnetrons by utilizing plasma discharges where the purpose is creating highly ionized plasma with large amounts of ionized sputtered material [34]. The high degree of ionization of sputtered species

results with smooth and dense films [35] and enables control over their phase composition, microstructure [36] as well as mechanical and tribological properties. Furthermore, it has been studied that it is very beneficial for enhancing adhesion of the films and gives rise to uniform film deposition on complex-shaped substrates [37].

The power is applied to the cathode as short pulses (pulse on time between 5 –5000 μs in HiPIMS and the duty cycle is kept low (<5%). The pulse frequency is in the domain of 100 Hz to 10 kHz. According to the low duty cycle operation, there is sufficient time for the target cooling. The relation between discharge voltage and discharge current in HiPIMS is illustrated in Figure 6 which shows that the discharge voltage and current are approximately twice compared to those of DCMS. Higher voltage and current in HiPIMS leads to a higher ionized fraction of sputtered flux [38].

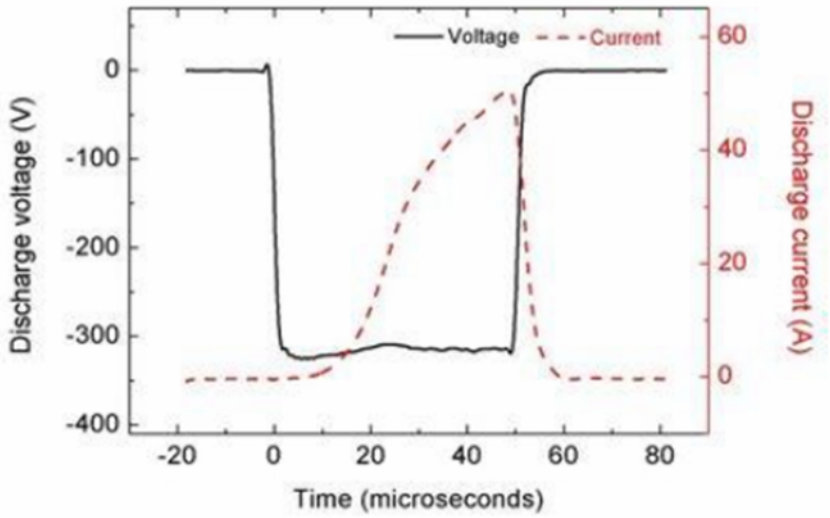

Figure 6: Current and voltage profile in magnetron sputtering [39].

Compared to DCMS, the ionized part of target particles is more than 50% in HiPIMS. Coatings deposited by HiPIMS are smooth and dense since ionized atoms have higher energies than sputtered atoms in a DCMS.

2.5 HiPIMS Plasma

Plasma is firstly described by Irvine Langmuir as a highly ionized state of matter which is quasi-neutral. Electrons, ions and neutral atoms or molecules are arranged in a way that positive and negative charges are nearly the same ($n_i=n_e=n_0$). In the case of highly ionized plasma, it is considered that the degree of ionization is high [26]. Plasma is made by discharging and an inert

gas such as Ar or Ne which is introduced into the chamber, shown in Figure 7. Substrate and chamber walls perform as an anode while the target serves as a cathodic electrode. Due to the collision of free electrons and gas atoms, breakdown in inert gas is initiated. In the plasma, ions are accelerated toward the target due to the positive charge of the ions. Generated ions are accelerated towards the target, collide with it and eject the target atom and directed onto substrate. Moreover, secondary electrons also are ejected by collision of ions with target which results in a self- sustained glow plasma [28].

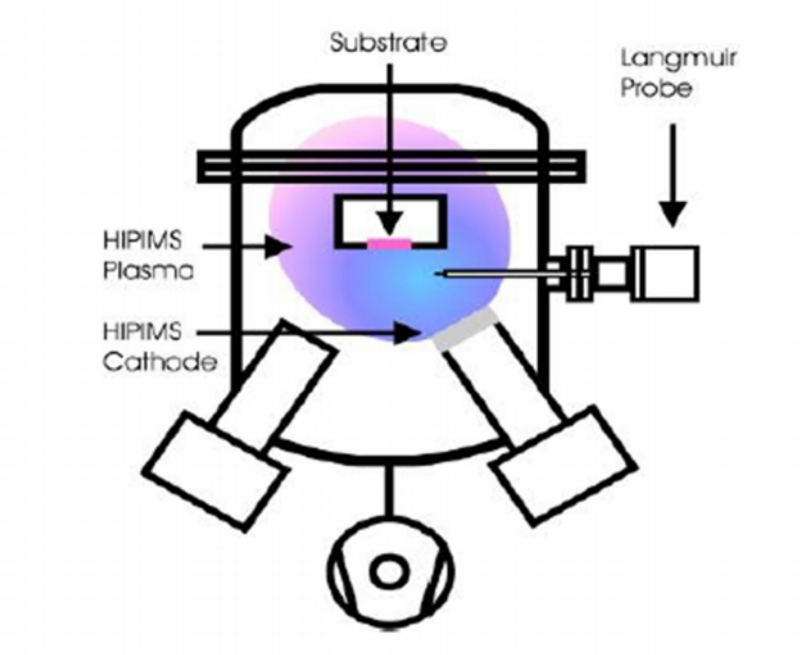

Figure 7: A deposition chamber scheme. Target is placed on the magnetron which is cathode in electric field. Plasma generation will be initiated at blue marked area in the picture [40].

Plasma is considered to be quasi-neutral in bulk. As electrons are lighter and mobile than other particles, electrons diffuse to the walls faster and voltage potential in the bulk of plasma (known as plasma potential) is initiated in the order of a couple of volts. Potential of grounded anode immersed in the plasma, such as chamber walls are held at 0 V. However, an isolated electrode immersed in the plasma is held at a negative potential. Therefore, in both cases, near the walls which interface with the plasma, there is a region with less amount of electron comparing to ions. Several studies have been carried out for adjusting the plasma density inside

the chamber by varying several process parameters and investigate the influence on the structure and properties of films.

2.6 DOMS

Deep Oscillation Magnetron Sputtering (DOMS) is a variant of HiPIMS which is used to obtain coatings with high sp^3 content and developed based on modulated pulsed power magnetron sputtering [41]. To achieve high target peak currents and voltages, it uses large voltage oscillation packets in long modulated pulses. The main parameters which can have a great impact on flux and energy of ions are working pressure, substrate bias voltage and current in DOMS.

There are two different sets of frequencies and data cycles of pulses. The first set is the frequency and duty cycle of modulation pulses which can be described by long modulation pulse-on and pulse-off times. Figure 8 shows 2 ms modulation pulse-on, 11.89 ms pulse-off time, the duty cycle of 14.4% and 72 Hz frequency.

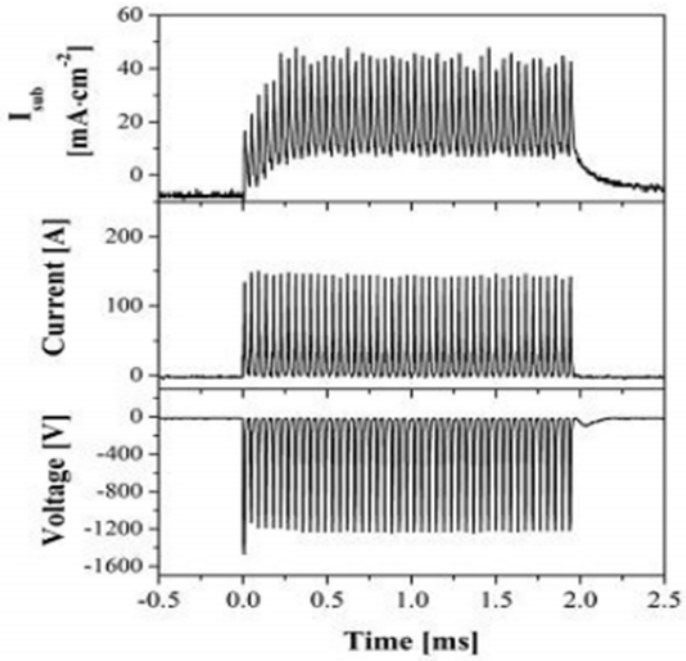

Figure 8: Voltage and Current oscillations waveforms of substrate in DOMS [42].

Modulated pulses which can be seen from Figure 8 contain several oscillation pulses with much lower pulse-on and pulse-off time which is the second set. Figure 9 indicates oscillation

pulses in the time from 0.50 to 0.60 ms with more details. The oscillation pulse-on and pulse-off time are 8 μs and 36 μs, respectively.

In DOMS, the fraction of sp^3 content depends on the energy level of the ion bombardment of the substrate. If the energy of the carbon ions is too much, the atoms rearrange their structures and make sp^2 bonding. Thus, to have a great amount of sp^3 content, there must be an optimum amount of energy [12].

Lin et al. [42] reported that using the DOMS technique for depositing DLC makes denser films and hardness of films can reach 35 GPa. Additionally, the influence of several process parameters on adhesion and stresses has been studied as well. The presence of hydrogen gas, variation in discharge gas pressure, presence of different interlayers and addition of alloying elements have significant effects on the film properties.

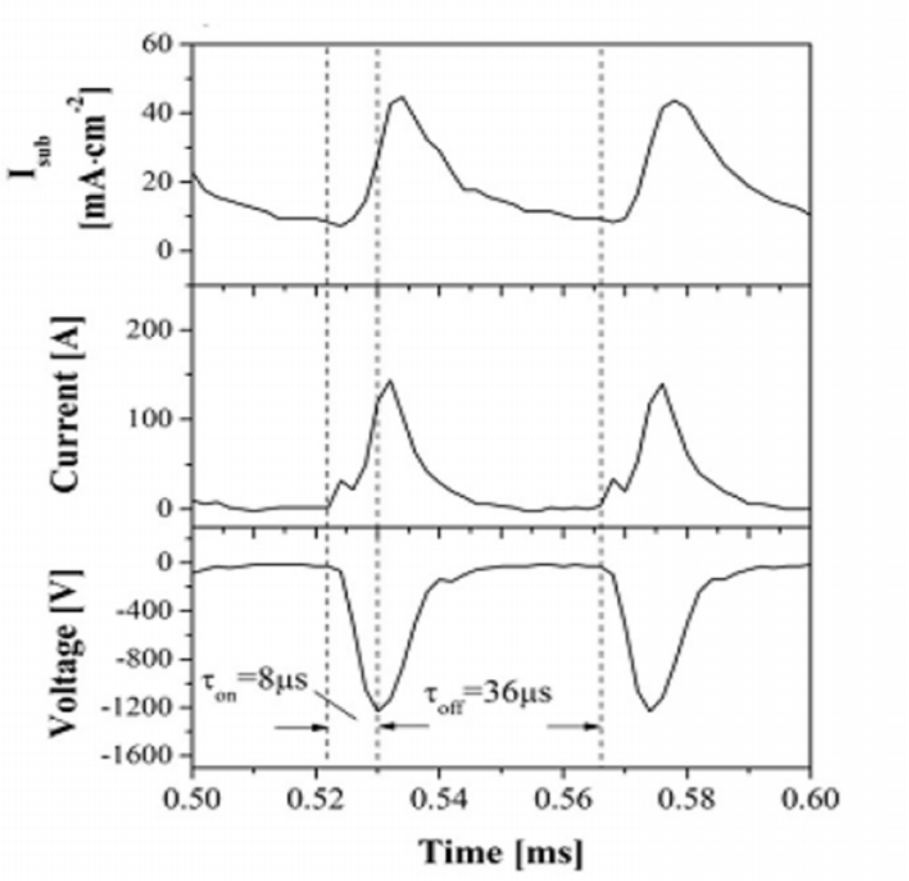

Figure 9: Oscillation of Voltage and Current within modulation pulse [42].

2.7 Tribological characteristics of DLC coatings

Most of the studies have demonstrated that DLC coatings have attractive chemical stability, mechanical and tribological properties (e.g. high hardness, low friction, high wear resistance, etc.) [43]. Thus, DLC films have been proposed for several tribological applications. However, properties of these coatings are dependent on depositions techniques and conditions, mating materials, sliding conditions. DLC coatings show the coefficient of friction less than 0.2 in atmospheric conditions [44]. The coefficient of friction values of DLCs are more or less the same in the case of unlubricated contacts against steel counterparts. Also, outperforming is noticed in the wear resistance of DLC against wear-resistant material and coatings in sliding contacts. Wear rates of DLCs are two or three orders of magnitude lower than compared to other coatings [17]. Hydrogen free DLC coatings show different tribological performance depending on the bond structure. Ta-C films reveal quite stable friction performance in humid environments, the values of CoF are typically 0.1-0.2 against different materials. On the other hand, the wear rates typically vary from 0.001 x 10^{-6} mm^3/Nm to 0.1 x 10^{-6} mm^3/Nm depending on the deposition technique and parameters used during deposition. Whereas, a-C films have higher wear rates than those of ta-C films.

In the research of Hirvonen et al. [45], ta-C films were deposited by an ion beam deposition method. The steady-state friction coefficient was observed on pin-on-disc tests which were conducted in ambient air. The values of friction were 0.14 and 0.06, against steel and silicon nitride, respectively. The wear rate of ta-C coatings was around 0.07 x 10^{-6} mm^3/Nm. The coatings deposited by pulsed vacuum arc-discharge technique which was composed of 66% sp^3 fraction and showed very high hardness (54 GPa) and Young's modulus (445 GPa) and wear rates were in the range of 10^{-9} to 10^{-10} mm^3/Nm.

Ronkainen et al. [46] studied the friction behavior of ta-C films with different applied loads (5-35N) and sliding velocities (0.1-3.0 $ms^{-1)}$. They found that the coefficient of friction exhibit fairly stable values in the range of 0.14-0.19 against steel pin and 0.1-0.19 against Al_2O_3 in humid air. The combination of high sliding velocity (2.6 ms^{-1}) and high load (35 N) showed the highest friction value (0.23). The cause of this was probably high generated temperature in the contact as it was verified by flash temperature calculations (T_f =700°C). Due to high temperature, the amount of water vapor in the sliding contact decreased which caused a rise in friction value.

Chapter 3: Experimental Methods

3.1 Experimental deposition details

3.1.1 Sample preparation

High-speed steel disc (2.5 cm diameter) and Silicon 100 (2x2 cm) were used as substrates for depositing DLC coatings. To obtain smooth surfaces for deposition, steel substrates were firstly polished with sandpapers and then both steel and silicon substrates were cleaned in an acetone and ethanol ultrasonic bath for 10 minutes each. They were then glued with silver glue (99.9 % purity) onto rotating aluminum substrate holder revolving at 23.5 rev/min around the central axis of the deposition chamber.

3.1.2 Deposition Chamber

The deposition chamber used in this work is shown in Figure 10. It was the cubic shape and manufactured with high-grade stainless steel with 400 x 400 x 400 mm dimensions. Along two adjacent walls inside of the deposition chamber, two cathodes were placed where one was on the fixed position and the other one was on the adjustable position. The cathodes were cooled with water through the set of tubes. For cleaning the target before deposition, a shutter was found inside the chamber which played a role as a barrier between target and substrates.

In this research, two targets with the same dimensions (150 x 150 mm and 10 mm thickness) were used which were a pure graphite (99.95%) and a pure chromium (99.99%). The fixed cathode was utilized for Cr deposition while adjustable one for C deposition. In all of the depositions, cathodes were located at an 8 cm distance from substrates. A base pressure lower than $3x10^{-4}$ Pa was obtained before all depositions by using a system which consists of a rotary and a turbomolecular pump.

DLC coatings were deposited on the substrates by using a DOMS power supply (HiPIMS Cyprium TM plasma generator, Zpulser Inc.). However, chromium interlayer was deposited by using a D.C. power supply and sputtering was carried out in the presence of pure Ar (99.999%) discharge gas.

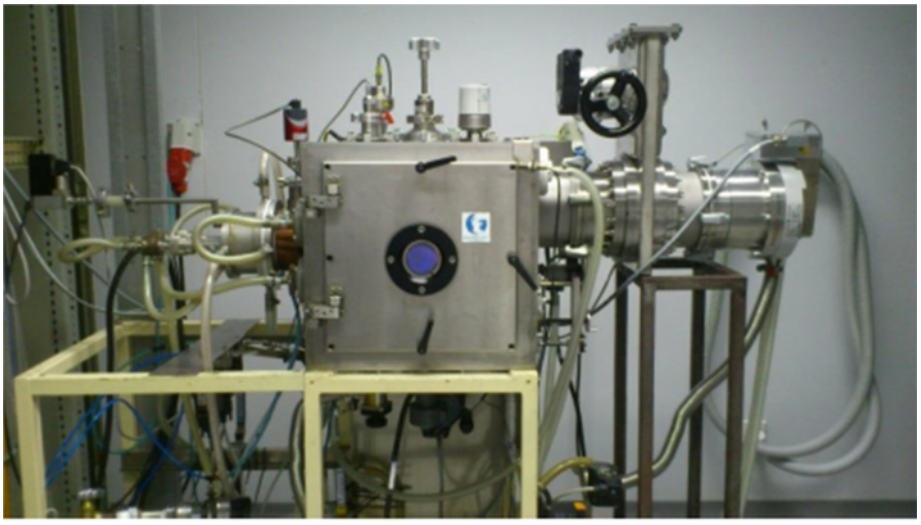

Figure 10: Deposition chamber

3.1.3 Deposition of DLC coating in DOMS mode at different t_{off}

Both substrates (Steel, Silicon) and targets (Cr, C) were cleaned adequately before all depositions for eliminating dust particles and impurities from the surface of the samples. In order to clean the C target, the DOMS power supply was used. Cleaning of Cr target and substrates carried out at the same time and D.C. power supply and pulsed power supply were used respectively. Parameters used during the cleaning process are listed in Table 1.

Table 1: Preparations of substrate and targets, prior to the deposition process.

Cleaning process				
Process	**Time (mins)**	**Sample**	**Power source**	**Voltage**
Target Cleaning	5	C target	DOMS	1410
Target Cleaning	60 (At the same time)	Cr target	D.C. supply	350
Substrate Cleaning		Steel and Si	Pulsed supply	370

After the initial cleaning processes, depositions of Cr interlayer, CrN interlayer were deposited in order to obtain good adhesion prior to the main DLC layer. Initially, an interlayer of Cr deposited for 10 minutes and then N_2 gas was introduced to the chamber and increased step by step until reaching the proper level to be able to deposit CrN interlayer (5 minutes). Then, the deposition of DLC coatings was done for 60 minutes by using – 80 V of bias.

Different t_{off} was applied in the deposition process for studying its effects on the DLC coating structure, tribological and mechanical properties. Two series of depositions were carried out, at 0.4 Pa and 0.8 Pa working pressures, accordingly. Deposition time (60 mins), substrate bias (-80 V) were the same for all depositions. Table 2 shows DLC deposition parameters for the series at 0.4 Pa and Table 3 shows the DLC deposition parameters for the series at 0.8 Pa.

Table 2: Deposition parameters for the coatings deposited at different t_{off} at 0.4 Pa.

t_{off} (µs)	Vp(V)	Ip(A)	Pp(kW)
44	1211	21.1	25.5
64	1215	20.8	25.3
84	1280	22.5	28.8
104	1260	21	26.5
124	1240	20	24.8

Table 3: Deposition parameters for the coatings deposited at different t_{off} at 0.8 Pa.

t_{off} (µs)	Vp(V)	Ip(A)	Pp(kW)
44	1411	53	74.8
64	1395	55	76.7
84	1420	52	73.8
104	1421	51	72.5
124	1410	51	71.9

The t_{off} was the same for the cleaning process and interlayer deposition in all depositions. It was just changed in the starting of DLC deposition automatically by programming in HiPIMS software without stopping the process.

3.2 Characterization techniques

3.2.1 Scanning Electron Microscopy (SEM)

A scanning electron microscope (SEM) is one of the methods for getting microscopic images of microstructure and morphology of materials. Sample images are generated as a sample is irradiated with a fine electron beam. Various interactions occur as the beam reaches and get into material which results with the emission of photons and electrons from or near the sample surface. For acquiring images, signals that are produced from the electron-sample interactions are detected with various types of detectors [47].

Two types of signals which are secondary (SE) and backscattered electrons (BSE) are used for inspection of the surface of a material. The secondary electron emission signal is the most widely used signal produced by the interaction of the primary electron beam with the specimen. SEs are created as a result of inelastic collision which occurs by scattering of incident electrons with specimen electrons. Due to the striking of the sample surface by the primary beam, ionization of specimen atoms occur and electrons which are loosely bound can be emitted and these are referred to as secondary electrons. Since they have relatively low energy (an average of around 3–5 eV) they can only escape from a region within a few nanometers of the material surface. Thus, SEs are able to mark the position of the beam precisely and give topographic information with good resolution [48].

An elastic collision and scattering phenomenon between incident electrons and specimen nuclei and electrons result with BSE. BSE has relatively higher energy which can be generated further from the surface and able to provide both compositional and topographic information.
Regardless of having several types of signals generated from a specimen, the x-ray signal is generally the only other signal which is used in SEM. The x-ray is generated due to recombination interactions between free electrons and positive electron holes. The x-ray signals allow for the determination of elemental composition through EDS (energy dispersive x-ray spectroscopy) [49].

SEM analysis was carried out in Zeiss (Merlin-61-50) equipment which equipped with FEG (Field Emission Gun). Images were captured from the surface at 1000X, 25000X and 50000X magnifications at different locations in order to study morphology and compactness of coating. For determining thickness and microstructure of coating and interlayer, the micrographs

were captured across coating's cross-section at 30000X magnification. EDS analysis was done in order to determine the elemental composition of the coating. The investigation was performed at various locations for determining the uniformity of the coating.

3.2.2 Atomic Force Microscopy (AFM)

Atomic force microscopy (AFM) is a scanning probe technique which uses different kinds of intermolecular forces as the detection signal in order to characterize the topography of surfaces of materials with nano-scale resolution [50]. Besides topography, stiffness, affinity, or adhesion properties can be obtained relatively easily. In AFM, a sharp tip is made of Si/Si_3N_4 mounted to end of the flexible cantilever and scanned over a sample surface. Basically, AFM uses Van der Waals force between the tip and the sample surface. Due to interaction forces between tip and surface, the deflection of cantilever occurs when the tip approaches a sample surface. The deflection of the cantilever can be sensed by a position-sensitive detector. A laser is directed onto cantilever which is then synchronously reflected back to a photo-detector that provides a feedback signal to piezoelectric scanners that maintain the cantilever tip at constant height or force. Thus, information about the surface roughness or interaction force between the sample and the tip is obtained. AFM analysis can be done in three different modes (1) contact mode, (2) noncontact mode, and (3) tapping mode depending on the type of interaction of the cantilever tip with the surface [51].

In this work, AFM measurement was carried out in a Bruker Innova equipment in a contact mode using SiN tip with radius lower than 10 nm. Firstly, a scan was carried out in a 10x10 µm and then two best locations were chosen and scanned in a 3x3 µm pattern.

3.2.3 X-ray photoelectron spectroscopy

X-ray photoelectron spectroscopy (XPS) which is also known as electron spectroscopy for chemical analysis (ESCA) is a quantitative technique in order to measure the elemental composition of the surface of a material as it normally probes to a depth of 10 nm. It also can be used for the determination of the binding states of the elements [52]. In this technique, substrates are bombarded with X-rays with defined energy. The X-rays interact with core electrons around the nucleus of various atoms that are in the sample and when these electrons are emitted from the sample they have well-defined kinetic energy which is given by:

$$E_k = h\nu - E_b - \emptyset$$

where hv is the X-ray photon energy, E_b is the electron binding energy and $\emptyset$ is the work function that is the energy needed for the electron to free itself from the surface. The kinetic energy of photoelectrons which are emitted from different atoms and orbitals and even the same type of atom and orbital in different binding states have different binding energies. Thus, types of atoms in the surface and their abundance can be determined by separating the electrons with different kinetic energy in an analyzer and displaying the results in a spectrum showing the photoelectron intensity as a function of kinetic energy [53]. Generally, typically, the Kα X-ray radiation from magnesium (1253.6 eV) or aluminum (1486.6 eV) is utilized for analysis. Determination of the energy of ejected electrons is typically done by a velocity analyzer such as a cylindrical mirror analyzerThe photoelectrons can be emitted from all electronic levels but the ones from outermost electronic states have energies that are sensitive to the chemical bonding between atoms. Chemical bonding information can be acquired from the photoelectron emission spectra by noting the "chemical shifts" of the XPS electron energy positions [54].

For all samples fast wide range spectra were initially acquired in order to see all elements and their peak positions. Subsequently, detailed spectra of each peaks were obtained. The main purpose of XPS measurements was to evaluate sp^3/sp^2 fraction in DLC films. All the measurements were done without previous ion bombardment of the films surface in order to avoid modifications of their local structure during the cleaning process. Tests were done at CEMUP by using Kratos Axis Ultra HAS equipment.

3.2.4 Nano – Hardness

A hardness test is usually carried out by a pressing specific shaped and loaded object (indenter) onto the surface of the material. The values of hardness are determined by measuring the depth of indenter penetration or by measuring the size of the impression left by an indenter. Nano- indentation hardness tester (MicroMaterialsNano Tester) was used in order to measure the mean hardness of the deposited films. All tests were carried out with a Berkovich tip where applied load was 5 mN. In order to get statistical value, 16 hardness measurements were performed for each sample.

3.2.5 Pin-on-disc

The coefficient of friction and wear rate of DLC coatings were evaluated by using the pin-on-disc (homemade) device. Pin-on-disc consists of a flat, pin or ball which is connected to a

stiff elastic arm that is put onto the test sample with some accurately known load. The sample is rotated at a selected speed. The friction force is evaluated by a load cell and transferred to the computer. The coefficient of friction is obtained from the test and presented against revolution or sliding distance. A fixed contact point and a stable position in the friction track formed by the pin on the sample is ensured by the elastic arm. The determination of the coefficient of friction is done by measuring the deflection of the elastic arm or by direct measurement of the change in the torque by a sensor located at the pivot point of the arm. Wear rates are calculated from the volume or weight of material removed during the test [55]. Experimental parameters for pin-on-disc are shown in Table 4. The material of counterpart (ball) used in tests was 100Cr6.

Table 4: Parameters for pin-on-disc experiment.

Load (N)	Rotation speed (rev/min)	Rotation radius (m)	Number of cycles	Temperature (°C)	RH (%)
5	159.2	0.006	160200	25	65

3.2.6 2D profilometry

2D profilometry is a technique that is typically used to measure two-dimensional topography of thin film surfaces. In this work, profilometer Mitutoyo surftest SJ-500 with diamond stylus tip was firstly used to evaluate residual stresses on the DLC coatings. Stylus tip physically touches the surface and moves across it and the vertical displacement of the stylus is converted to a height value by force feedback. The process of conversion involves some electronic and mechanical devices [56]. The test was performed on a 17mm of 20 mm DLC coating. Evaluation of wear rate after pin-on-disc experiment was done by this technique as well.

Chapter 4: Results and Discussion

In this section, the effect of the t_{off} experimental parameter on the DLC films properties is studied at two different deposition pressures (0.4 and 0.8 Pa). DLC films which were deposited using different values of t_{off} and subsequently analyzed from the point of view of their microstructure and mechanical and tribological properties.

4.1 DLC films deposited by DOMS at 0.4 Pa

4.1.1 SEM results as a function of t_{off}

This section includes the surface morphology and the cross-section of DLC coatings deposited at 0.4 Pa working pressure, different t_{off} by DOMS (Figure 11). As already mentioned in the experimental section, Cr and CrN interlayers with a thickness around 1 µm were deposited over the substrates. It can be observed from the cross section micrographs that the interlayer has an open columnar microstructure that is known to create tensile stresses which act to prevent compressive stresses upon DLC films deposition [57]. As can be seen from SEM micrographs from Figure 11, there is no major difference on the surface morphology of the films as t_{off} is increased from 44 to 124 µs. Regardless of the deposition parameters, all the micrographs present similar cauliflower-type morphology which consists of small grains that agglomerate to form larger protruding structures.

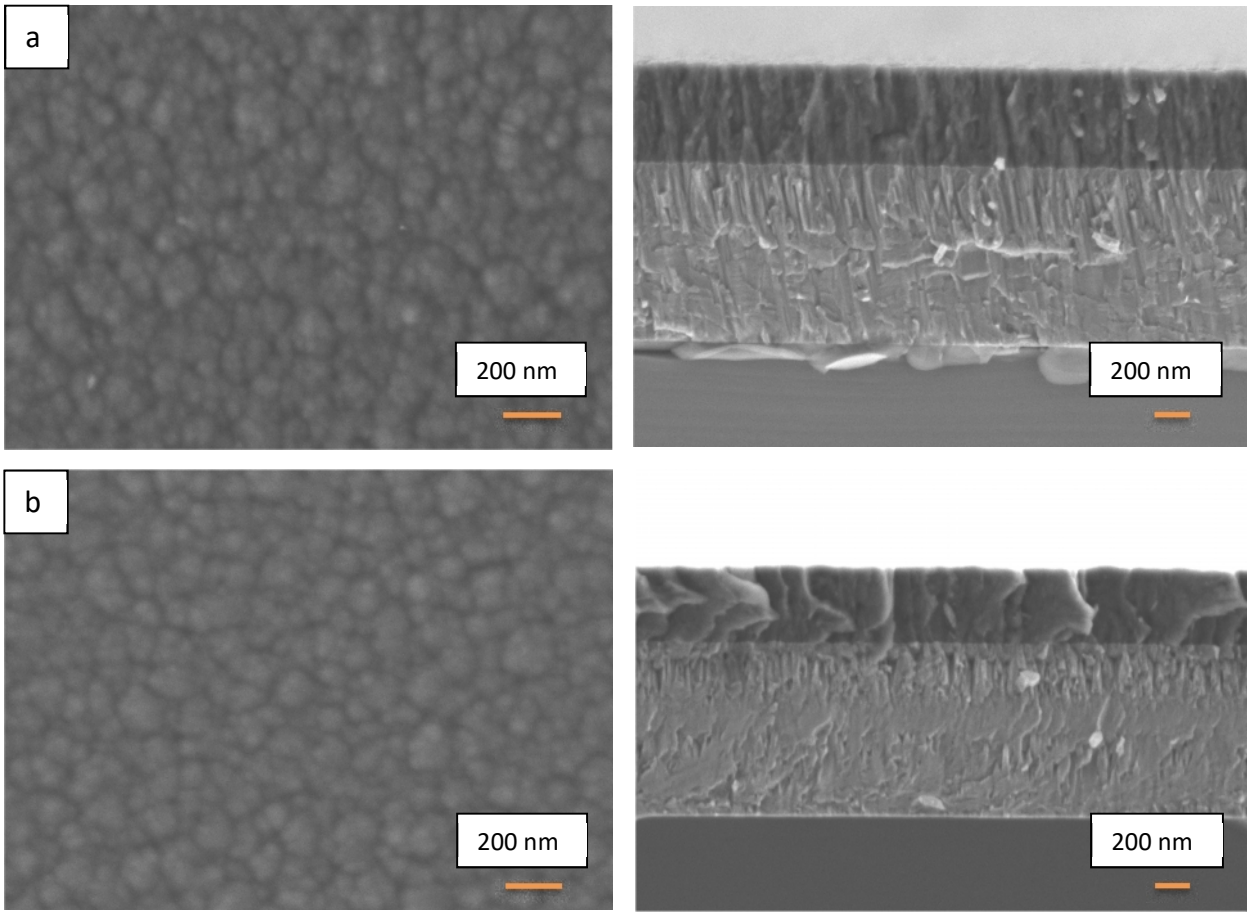

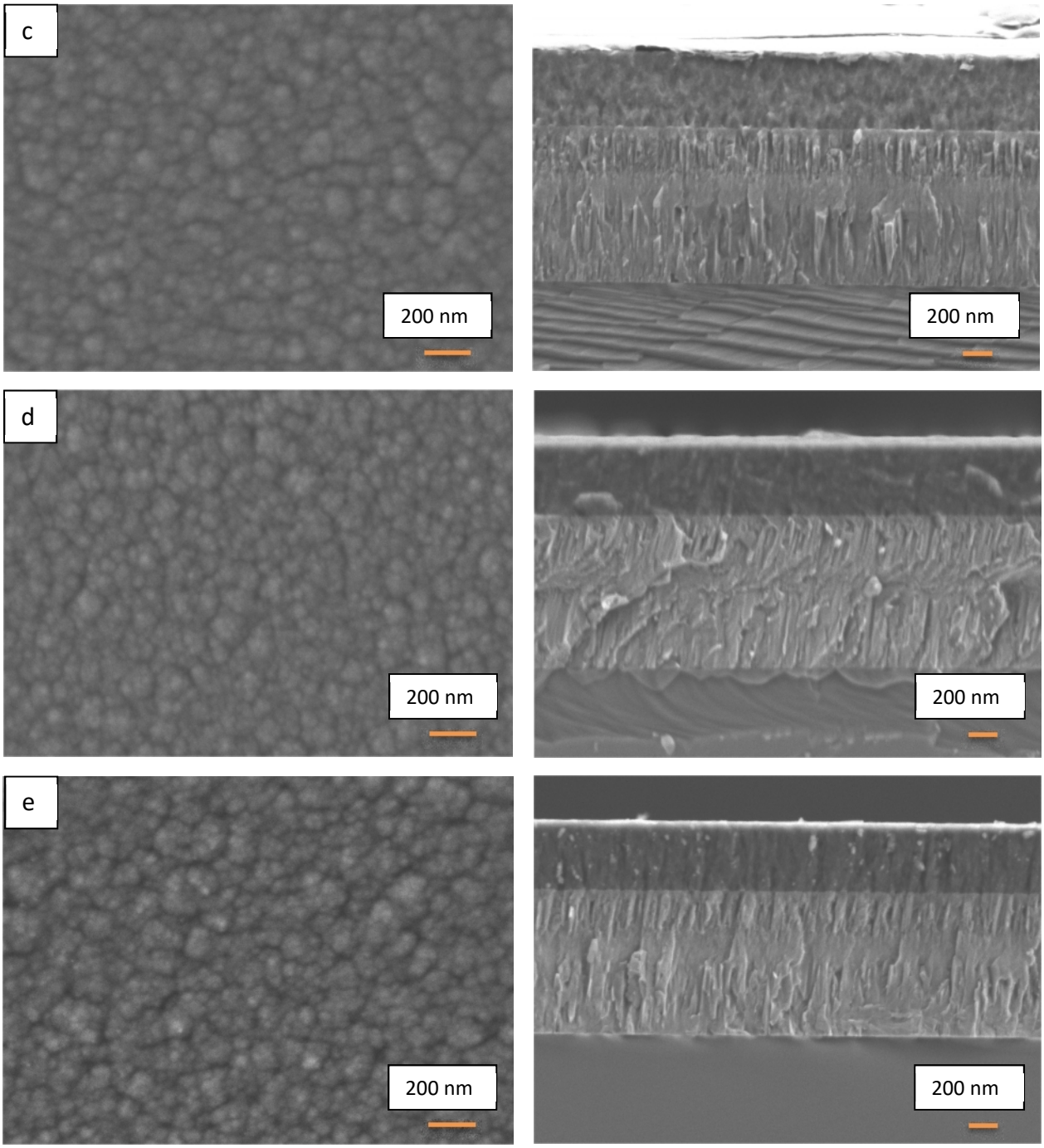

Figure 11: SEM cross-section and surface micrographs of the DLC coatings deposited by DOMS at 0.4 Pa , t_{off} of a) 44 µs b) 64 µs c) 84 µs d)104 µs; e) 124 µs

As optimum high substrate bias (-80 V) was applied, characteristic dimensions of the grains that agglomerate are very small due to high surface diffusion. The cross section micrographs of the films (Figure 11) show dense columnar microstructures irrespectively of the

values of t_{off}. Most of the features that can be observed on the DLC films cross sections arise from the breaking of the samples prior to observations.

The deposition rate of the DLC films deposited at different t_{off} is presented in Figure 12. Considerable differences are not seen in the deposition rate of coatings as t_{off} is changed, except the coating deposited at 64 µs where the deposition rate is significantly lower than others.

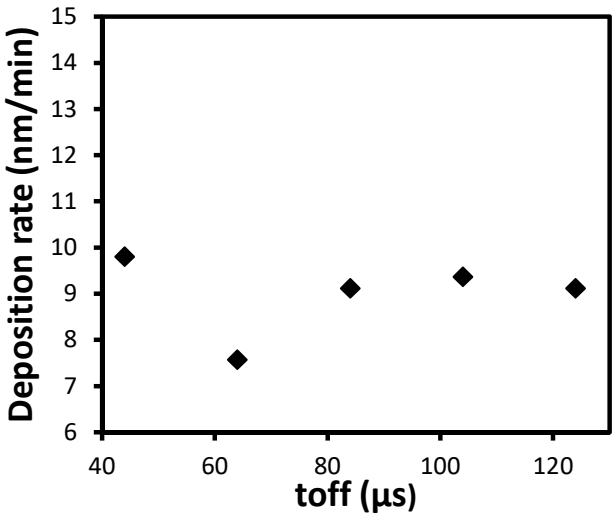

Figure 12: Deposition rate of DLC films deposited at different t_{off} , 0.4 Pa

4.1.2 AFM results as a function of t_{off}

The AFM surface scans of DLC coatings deposited at different t_{off} were obtained in order to investigate topography of the coating surface and evaluate the roughness. The AFM topographic images were acquired in contact mode within an area 3 by 3 microns.

In Figure 13, the AFM topography images of the DLC coatings deposited at 0.4 Pa with different t_{off} are presented. In agreement with the SEM results, the surface morphology of the films does not noticeably change with changing t_{off}. All the films reveal a granular surface morphology with small grains with similar dimensions irrespectively of the t_{off}. The formation of aggregates typical of the cauliflower type morphology observed in the SEM surface micrographs is much less obvious in the AFM surface images. Overall, differences in AFM images are not distinguishable, except image of coating deposited at 44 µs (Figure 13.a) which can presumably be due to experimental error or some imperfections on coating.

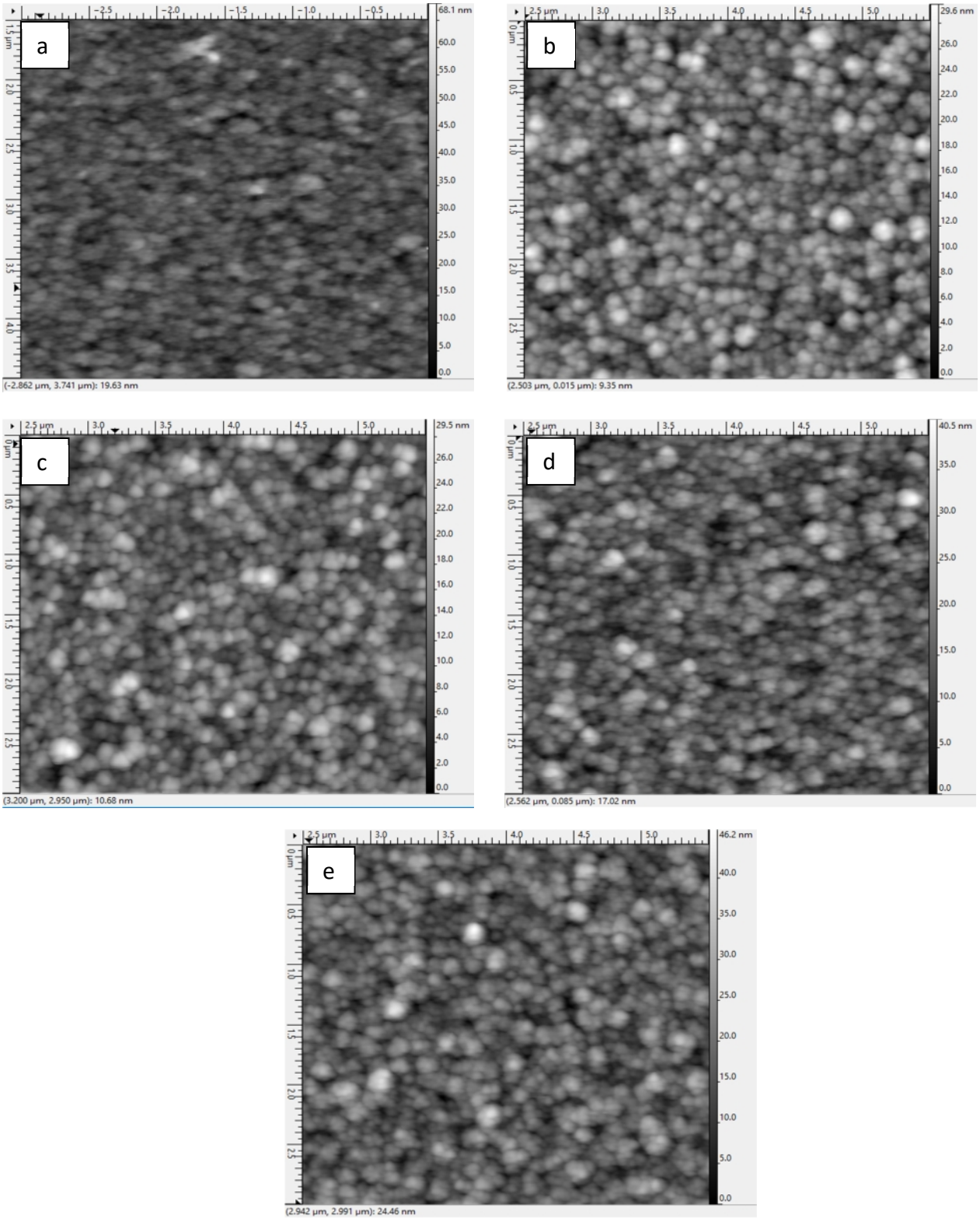

Figure 13: AFM images the DLC coatings deposited by DOMS at 0.4 Pa, t_{off} of a) 44 µs b) 64 µs c) 84 µs d)104 µs; e) 124 µs

In Figure 14, the mean roughness of DLC coatings deposited at different t_{off} is shown. It can be seen from the results that films are smooth since mean roughness (Ra) values are very low (between 3 and 4 nm). Generally, a low roughness can be explained by the use of a high substrate bias during the deposition process, as used in this work, since an increased bombardment of the film by the ionic species result in a smoother surface. The roughness evolution with t_{off} suggests a trend with a minimum at 84 µs although a conclusion about this is not possible due to the error margin of the measurements.

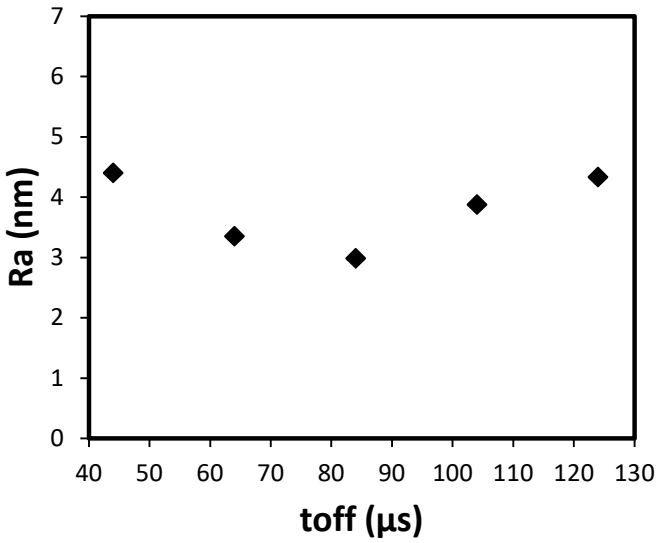

Figure 14: Roughness of DLC films deposited at different t_{off}, 0.4 Pa

4.1.3 Hardness results as a function of t_{off}

The hardness of the films was measured by Nano-indentation (MicroMaterialsNano Tester) using a Berkovich diamond indenter. Indentation load was 5 mN as already mentioned in experimental part.

The hardness and Young's modulus of the DLC films deposited at different t_{off} using DOMS is presented in Figure 15. Likewise the results from other techniques, hardness results also show fluctuation as t_{off} is increased. The highest hardness (19.4 GPa) is observed on the coating which is deposited with 84 µs. Other hardness values are lower than this and close to one another, but the lowest hardness is experienced as t_{off} is increased to 124µs.

Overall, hardness values are quite high in all of the deposited films. The main factor that has great influence on the hardness of DLC is sp^3 content. The strong and directional sp^3 bonding

of carbon atoms results in the formation of a three-dimensional (tetrahedral) network of σ bonds which increases the hardness of DLC films [58]. One of the deposition variables which has a major effect on the sp^3 fraction of DLC films is the substrate bias. The optimum substrate bias voltage for the DLC films deposited by DOMS (- 80 V) was already optimized in a previous work by Ferreria et al. [59]. The authors found that the hardness of the film deposited with a substrate bias of − 100 V was lower than that of the film deposited with a substrate bias of − 80 V. McKenzie et al. found that thermal spikes could be present when bombarding energies are very high [60]. The excess amount of thermal energy can lead to transition of sp^3 bonds to sp^2.

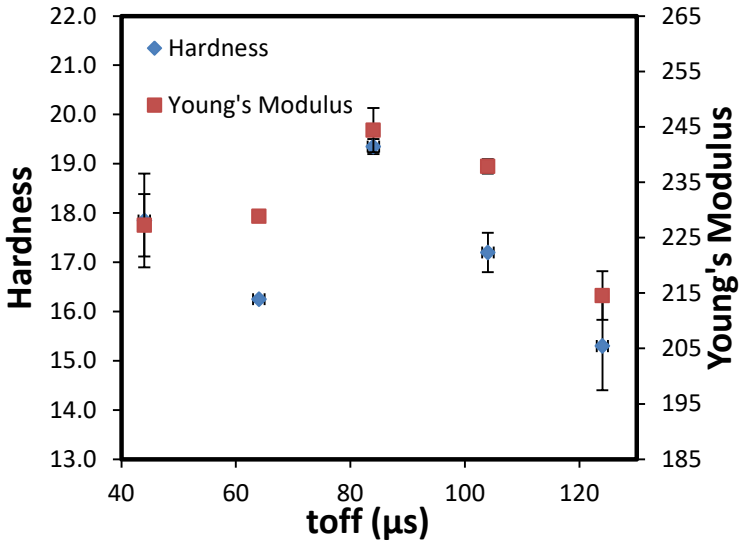

Figure 15: Hardness and Young's modulus of the DLC coatings deposited by DOMS at different t_{off} , 0.4 Pa

Besides the sp^3 bonding fraction, the microstucture and thus the density of the films also plays a critical role in determining the mechanical properties of the films. As the same bias was applied to all the deposited films, the highest hardness at 84 µs is probably related to a higher density of the coating.

The maximum depth reached during the nano-indention tests is shown in Figure 16. As expected, it shows the opposite trend compared to that of hardness. The hardest surface should exhibit the lowest value of depth as in the case DLC film deposited at 84 µs where maximum depth is around 104 nm. The biggest depth (116 nm) in these series is seen on film deposited at

124 µs. The maximum depth in indentation should be lower than 1/7 of coating, but it is evident that they are higher in these results. Therefore, it can be concluded that hardness results were somehow influenced by substrate.

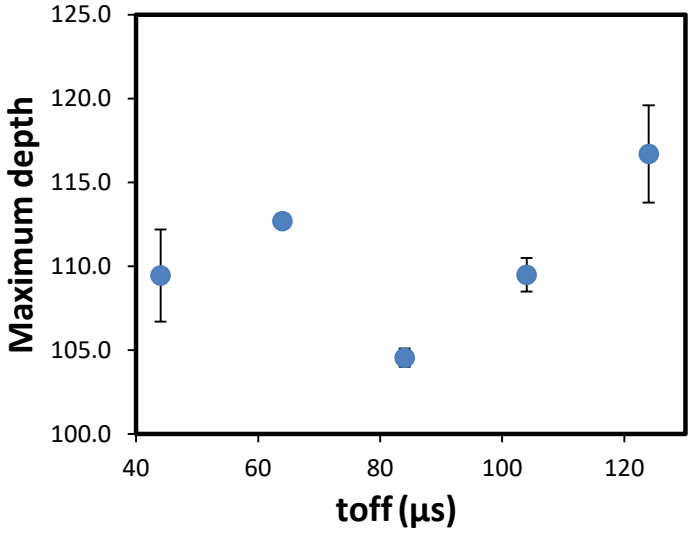

Figure 16: Max Depth of the DLC coatings deposited by DOMS at different t_{off}, 0.4 Pa

4.1.4 Tribological results as a function of t_{off}

The tribological properties of the DLC films, coefficient of friction (CoF) and specific wear rate, were evaluated by pin-on-disc tests. The CoF versus number of test cycles graph of the DLC coatings deposited at 0.4 Pa at different t_{off} is shown in Figure 17. All tests were done at room temperature and ambient conditions. An initial running-in period is seen in the beginning of the test, which is characterized by higher values of CoF. After this period, a steady state regime is seen where CoF is almost constant.

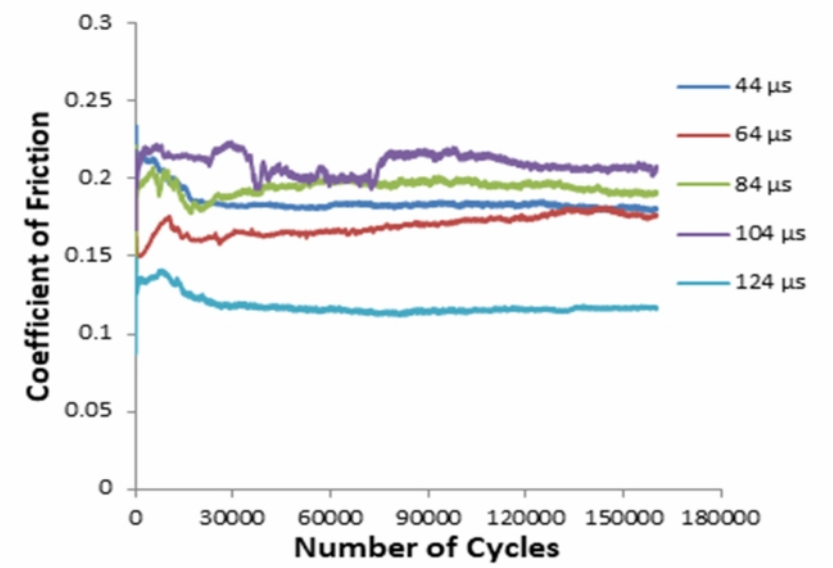

Figure 17: CoF versus number of cycles graph for DLCs deposited at different t_{off}, 0.4 Pa

The CoF of the films deposited at different t_{off} as calculated by averaging over the steady state regime and presented in Figure 18. It is noticeable from the results that there is an increase in the values of CoF (from 0.18 to 0.21) as t_{off} is increased from 44 µs to 104 µs with a slight decrease at 64 µs. As t_{off} is further increased, the coating deposited at 124 µs shows the lowest value of CoF (0.11). This result can be correlated with the lower hardness of this coating and should be due to a higher sp^2 fraction. The most important factor which plays a role in diminishing friction is graphitization phenomenon. Formation of graphite occurs on the top of the asperities in tribocontact and this graphite forms a layer with a low-shear strength which provides low friction [61]. Due to repeated sliding, some graphite is transferred into the tribofilm formed on the wear surface of the ball and collected in the sliding deposit in front of the tribocontact. In the tribocontact, tribolayer is formed on the wear surface of the ball which slides on the thin graphite layer. The tribolayer can act as chemically stable and inert layer which prevents direct contact between the graphite and ball. Tribological performance of DLC coatings is closely related to chemical and physical nature of the tribolayer. Under dry conditions, tribolayer mainly consist of carbon-rich interlayer with a low-shear strength, which can be transferred repeatedly back and forth between the two contact surfaces and contributes to low friction, and wear rate [62].

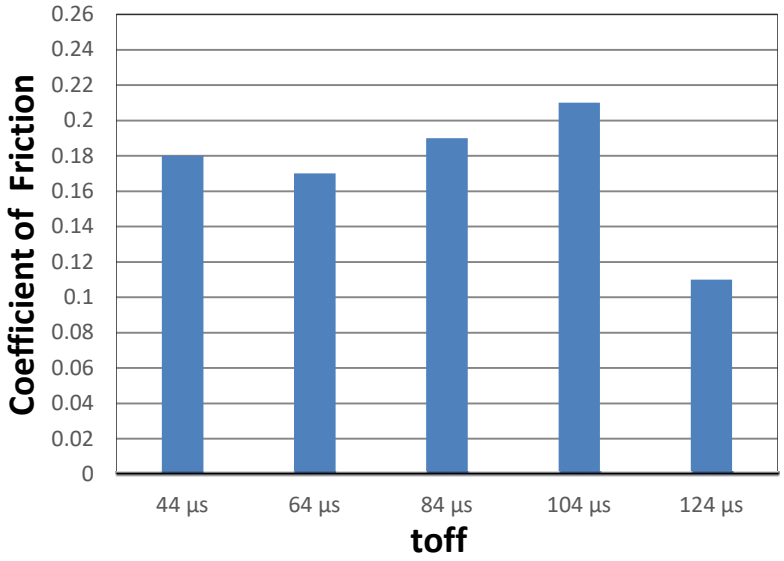

Figure 18: CoF as a function of t_{off} for DLC films deposited at 0.4 Pa

After pin-on-disc experiments, the wear rates measurements were carried out on worn steel samples by 2D profilometer. Figure 19 shows how does the increasing of t_{off} influences the specific wear rate of DLC coatings deposited by DOMS. The highest specific wear rates, around $0.7x10^{-16}$ m^3 N^{-1} m^{-1}, were obtained for the coatings deposited at t_{off} values of 44, 64 and 104 µs. The DLC film deposited at a toff of 84 µs has a lower specific wear rate of $0.55x10^{-16}$ m^3 N^{-1} m^{-1}, which correlates well with its higher hardness in comparison to the previously mentioned DLC films. The higher wear resistance of the film should be due to its higher sp^3 fraction. However, the lowest specific wear rate (0.42 $x10^{-16}$ m^3 N^{-1} m^{-1}) was obtained for the DLC film deposited at a value of toff of 124 µs, which has the lowest hardness value. In this case the wear rate of the films correlates well with its lower coefficient of friction and may be due to a slight increase of the film density as suggested by the SEM results.

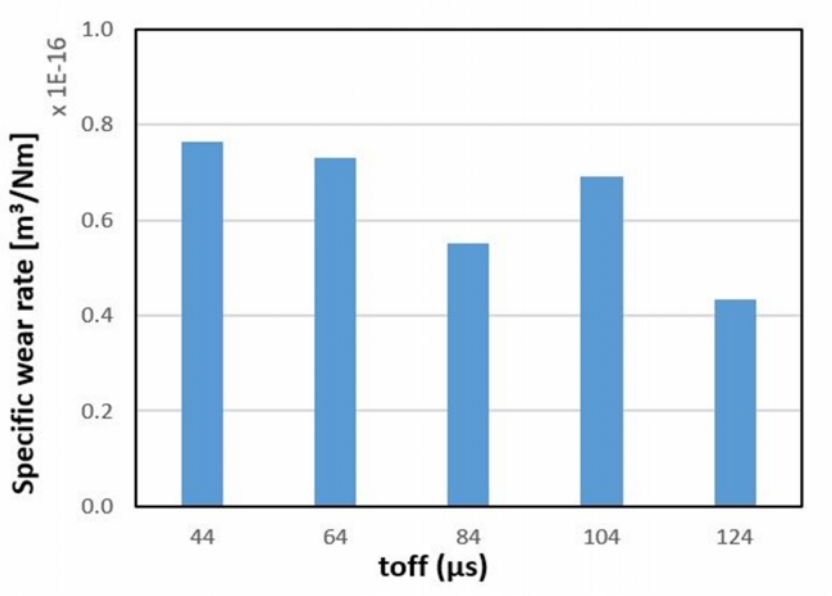

Figure 19: Specific wear rate as a function of t_{off} for DLC films deposited at 0.4 Pa

For further investigation, SEM was used in order to observe wear tracks which are left on the surfaces of DLC films and images of wear scar on the ball were captured by optical microscope (Figure 20). As fairly low load (5N) was applied in test on hard films, furrows on wear traces are not deep and overall seem very clean. No significant differences can be detected from the SEM micrographs as they show similar wear tracks with similar furrows and little amount of debris. Thus, severity of wear on the films cannot be well distinguished by SEM wear track micrographs. Overall wear tracks appear to be smooth without cracking, pits or plowing grooves, indicating excellent tribological properties of the films.

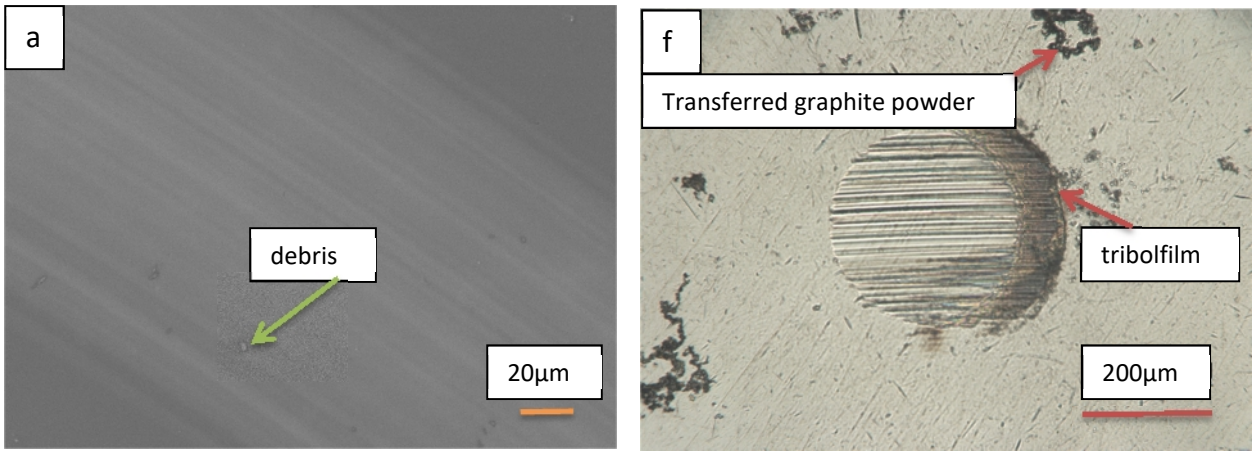

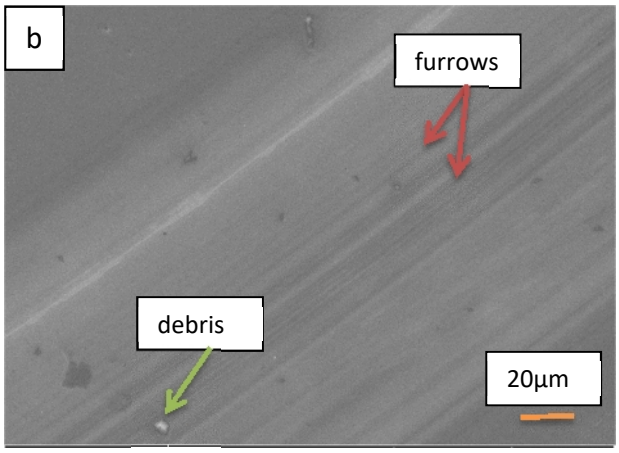
b
furrows
debris
20µm

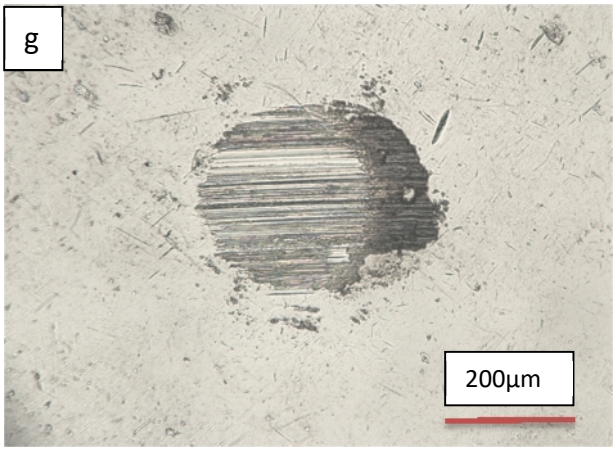
g
200µm

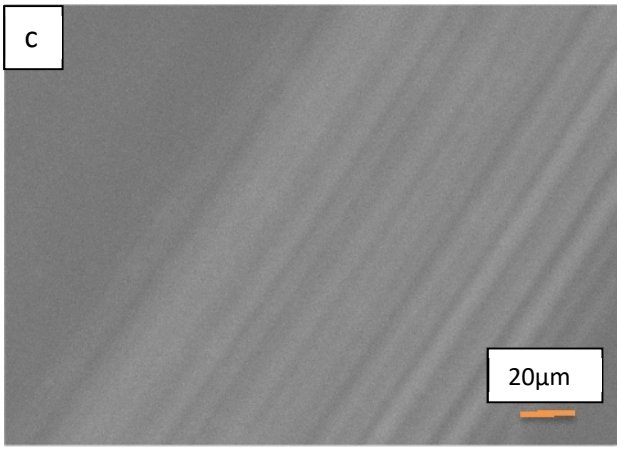
c
20µm

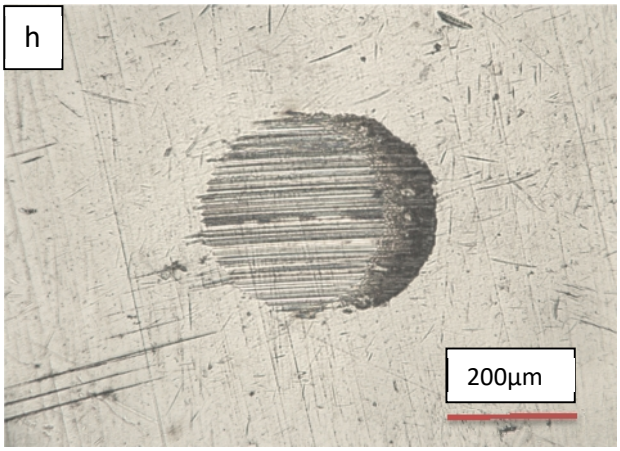
h
200µm

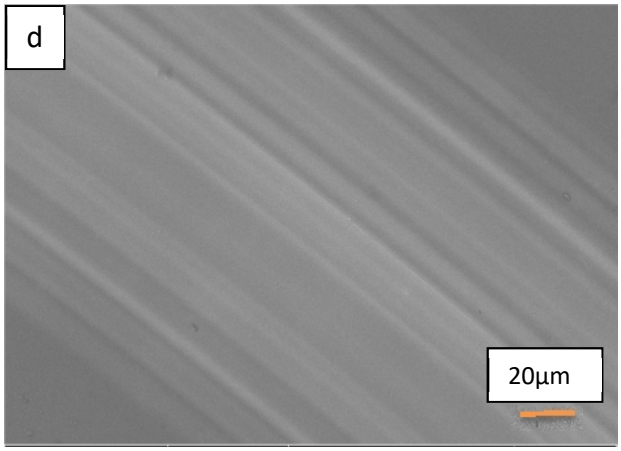
d
20µm

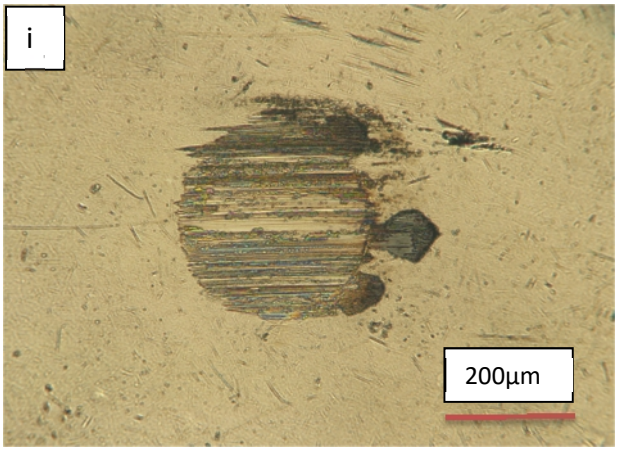
i
200µm

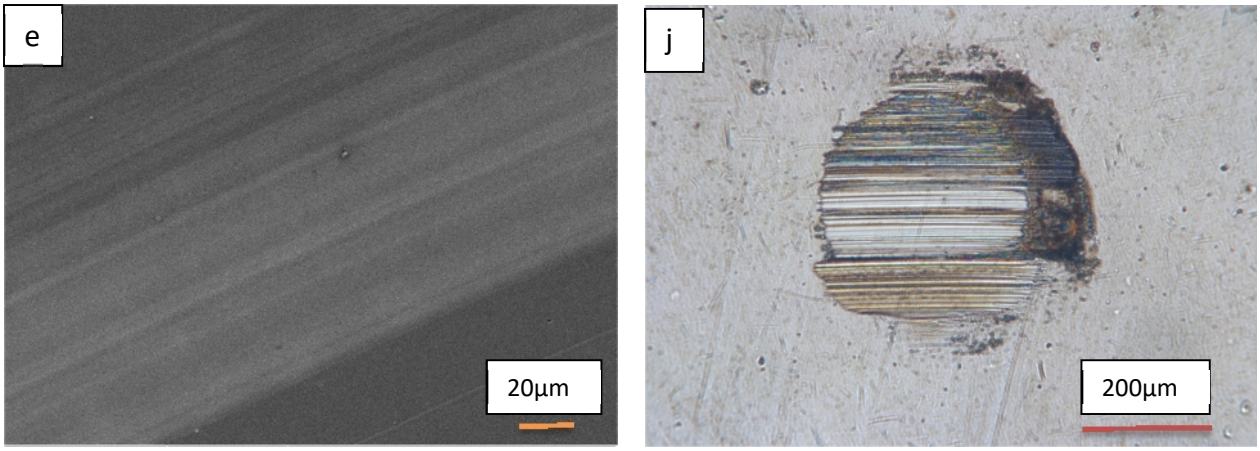

Figure 20: SEM wear track and wear scar images of the DLC coatings deposited by DOMS at 0.4 Pa and t_{off} of a) 44 µs b) 64 µs c) 84 µs d)104 µs; e) 124 µs

Images of the wear scars are shown in Figure 20 (f,g,h,i,j). Two optical microscope images (one before cleaning graphite powder, one after) were taken just upon completion of pin-on-disc test. Wear scar images that were taken after cleaning are presented in this work. Thus, the counterparts show only some vestiges of the transferred graphitic layer. The size, appearance (metallic or not) and depth of scratches of wear scar on the ball can be correlated with wear resistance of films. The counterpart of the coating that shows the highest wear resistance (t_{off} of 124 µs) seems to be more severely worn (Figure 20, j) as severe deep scratches and metallic appearance are observed.

4.1.5 Residual stresses as a function of t_{off}

During the DLC films deposition, the bombardment with higher energy of carbon and argon ions results in a shallow implantation usually referred as subplantation. This process originates a buildup of compressive stresses in the deposited DLC films. The amount of compressive intrinsic stresses depends on the impact energy per atom from a discharge containing energetic argon, carbon or hydrocarbon ions where typical energies are in the range from tens to a few hundred eVs [63]. The compressive residual stresses of the DLC films as evaluated by the substrate bending method are presented in Figure 21 as a function of t_{off}.

As can be observed in Figure 21, the evolution of the stresses with t_{off} does not show any noticeable trend. The average values of stresses at 84 and 104 µs are close to 0.5 GPa, respectively. The stresses vary between 0.15 GPA at t_{off} = 64 µs and 1.1 GPa at t_{off} = 64 µs. On the overall, the compressive residual stresses of all the DLC films are quite low in comparison

with the values of several GPa usually referred in the literature for this kind of coatings and should not compromise the performance of the films in service applications.

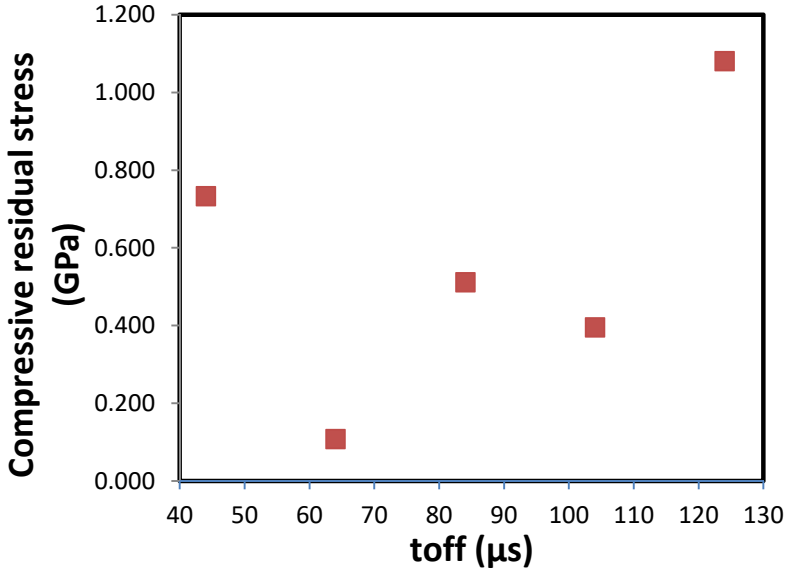

Figure 21: Compressive residual stresses as a function of t_{off} for DLC films deposited at 0.4 Pa

4.2 DLC films deposited by DOMS at 0.8 Pa

4.2.1 SEM results as a function of t_{off}

The surface morphology and the cross-section of DLC coatings deposited at 0.8 Pa working pressure by DOMS with different t_{off} values are presented in Figure 22. Since the interlayer (Cr and CrN) is the same for this series of coatings as for the coatings deposited at 0.4 Pa, it has similar open columnar microstructure independent on changing $t_{off.}$

Once again, the surface micrographs of the all DLC films deposited at 0.8 Pa reveal cauliflower-type morphologies consisting of small grains that agglomerate to form larger protruding structures. The surface morphology of the films does not significantly change with t_{off} although the defocusing of the micrograph of the film deposited at the highest t_{off} may indicate a small decrease of its surface roughness. The cross section of film deposited at 44 µs (Figure 22, a) shows a clearly columnar microstructure. Increasing t_{off} to 64 µs results in a much less columnar microstructure which is progressively replaced by featureless microstructure as t_{off} is further increased.

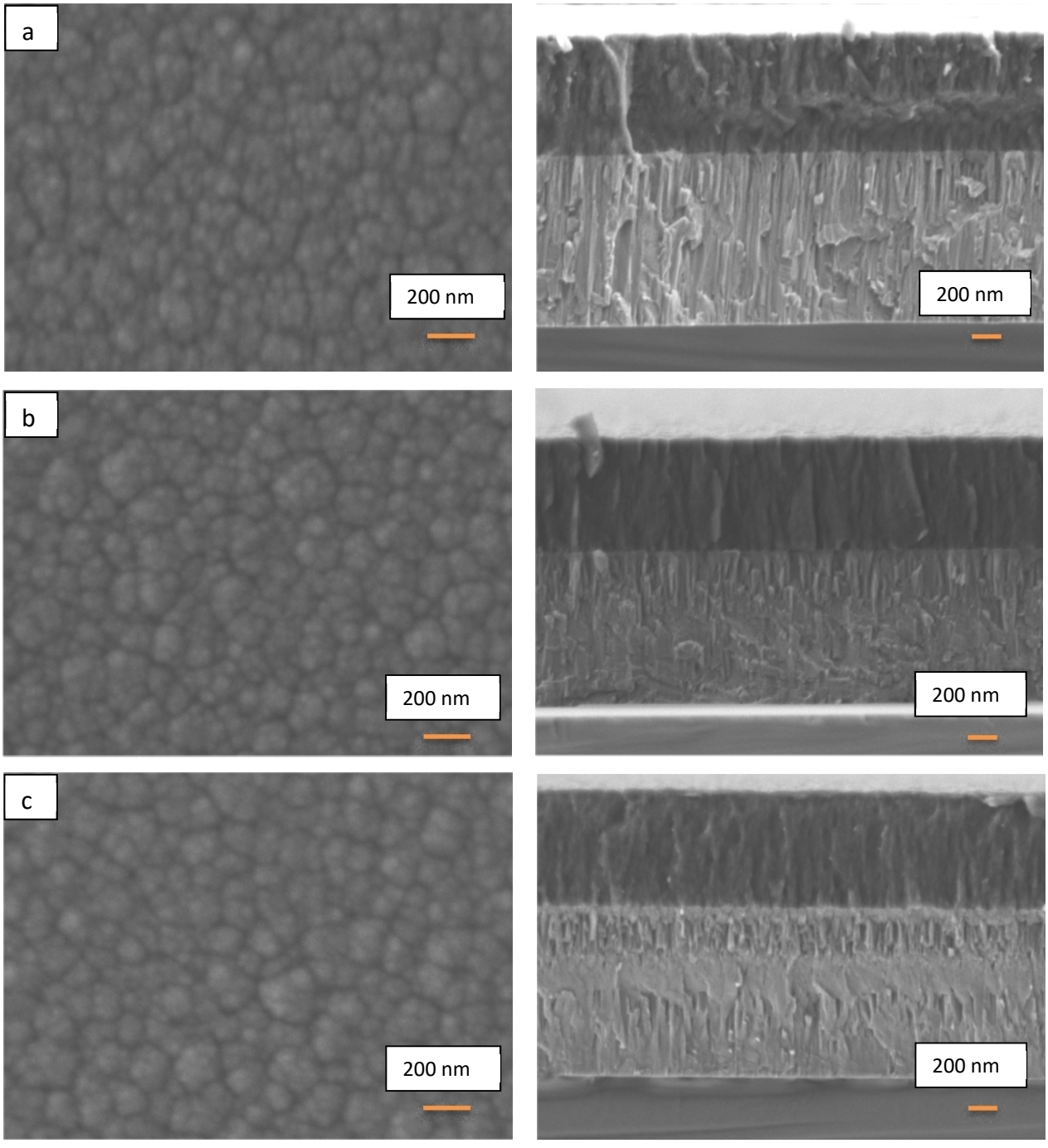
a
200 nm
200 nm
b
200 nm
200 nm
c
200 nm
200 nm

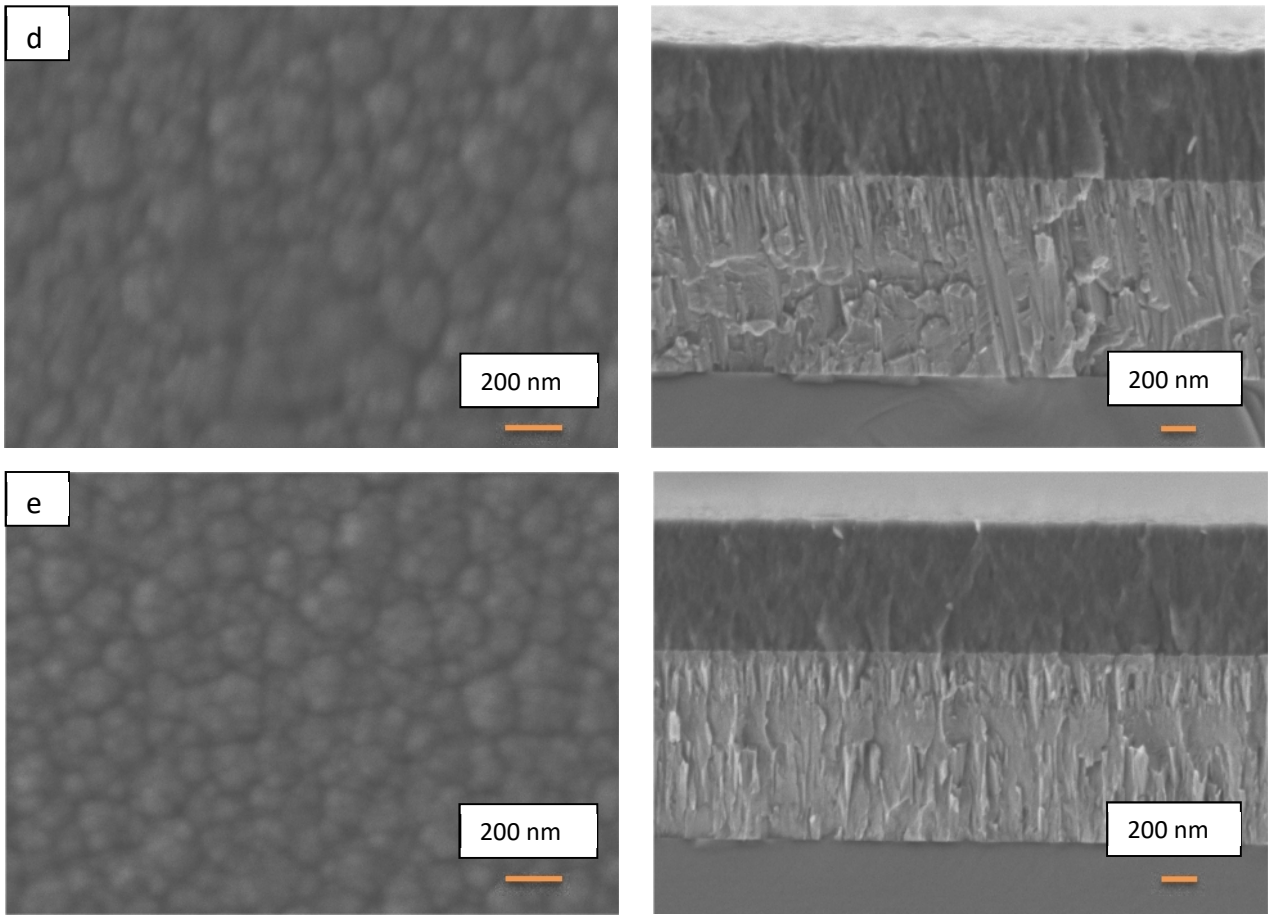

Figure 22: SEM cross-section and surface micrographs of the DLC coatings deposited by DOMS at 0.8 Pa and t_{off} of a) 44 µs b) 64 µs c) 84 µs d)104 µs; e) 124 µs

The deposition rate of DLC films deposited at a deposition pressure of 0.8 Pa is displayed in Figure 23 as a function of t_{off}. As t_{off} is increased from 44 to 124 µs, the deposition rate of films decreases from 14.2 to 12.8 nm/min. The deposition rate of the films deposited at 0.8 Pa is noticeably higher than that of the films deposited at 0.4 Pa.

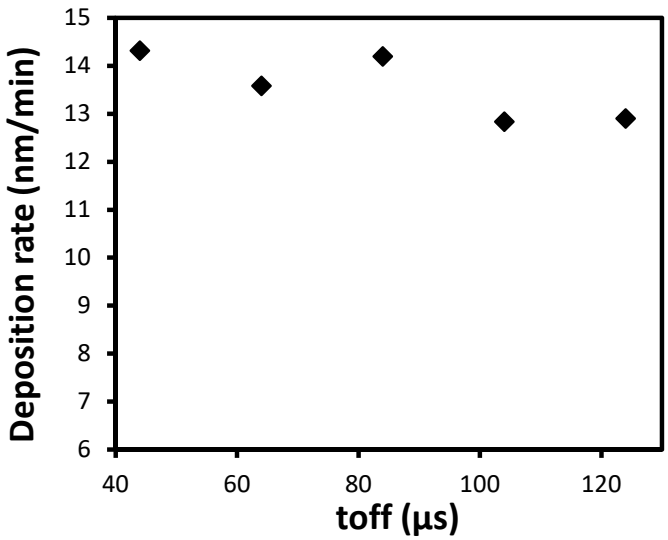

Figure 23: Deposition rate of DLC films deposited at different t_{off} , 0.8 Pa**.**

4.2.2 AFM results as a function of t_{off}

The AFM topography images of the DLC coatings deposited at 0.8 Pa at a different t_{off} are illustrated in Figure 24. Excepting the for the DLC film deposited at the lowest t_{off}, the AFM images exhibit similar surface morphologies for all coatings, just small variations on the grain sizes could be detected as t_{off} is changed. This result confirms the results obtained by SEM. The DLC film deposited at the lowest t_{off} exhibits a significantly lower size of the surface features. This result maybe be due to an experimental error as the characteristic dimensions of the surface features in the AFM image are significantly different in comparison to the corresponding SEM surface micrograph.

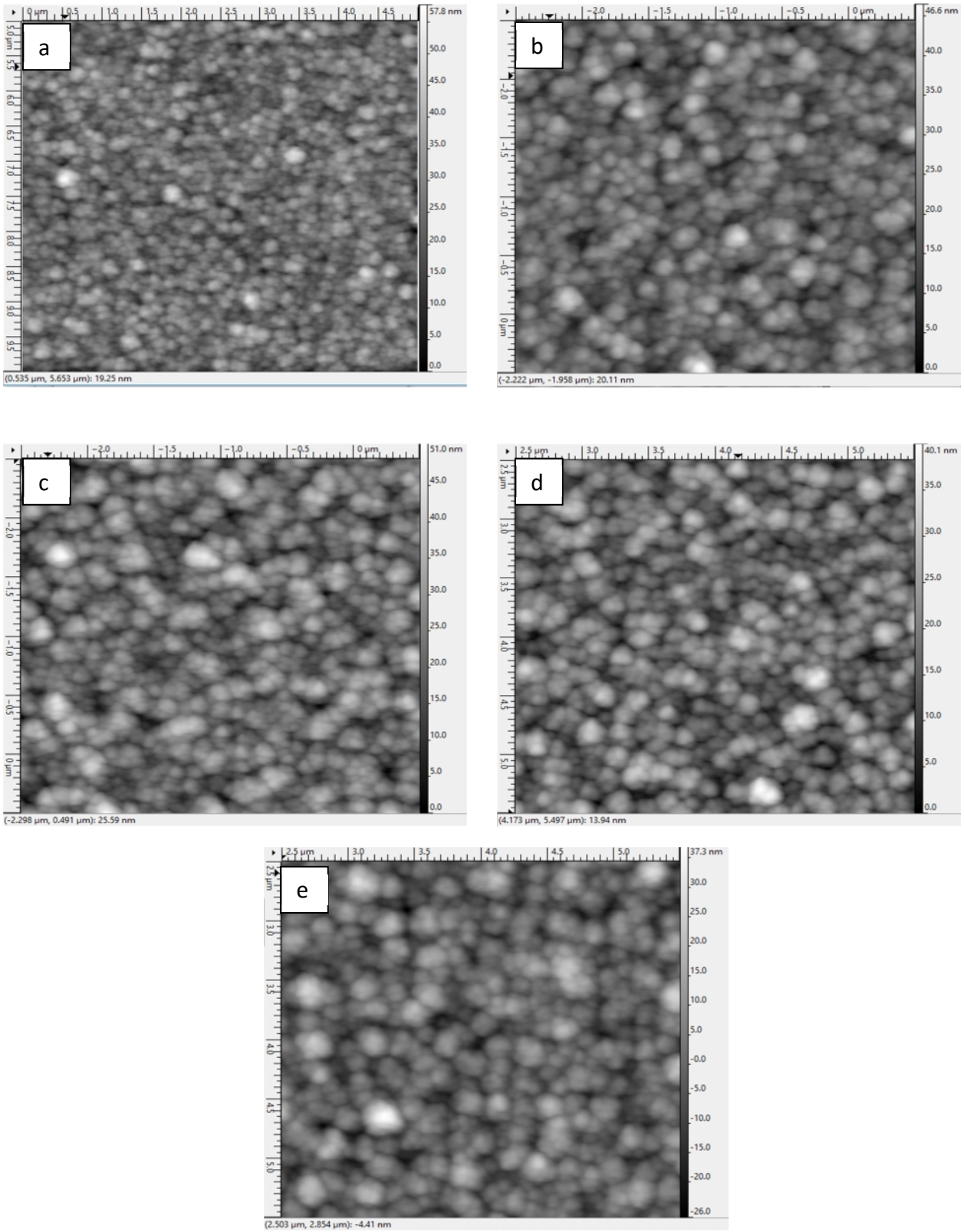

Figure 24: AFM images of the DLC coatings deposited by DOMS at 0.8 Pa, t_{off} of a) 44 µs b) 64 µs c) 84 µs d)104 µs; e) 124 µs

The mean roughness of DLC coatings is shown in Figure 25 as a function of t_{off}. On the overall, mean roughness values for the coatings deposited at 0.8 Pa are slightly higher than those of deposited at 0.4 Pa. This result can be explained by the higher thickness of the DLC films deposited at 0.8 Pa. The surface roughness is mostly determined by the shadowing effect which increases with increasing film thickness. The lowest roughness (around 4 nm) is observed at 64 µs, whereas the coating deposited at 124 µs shows the highest value of roughness, which is around 6 nm.

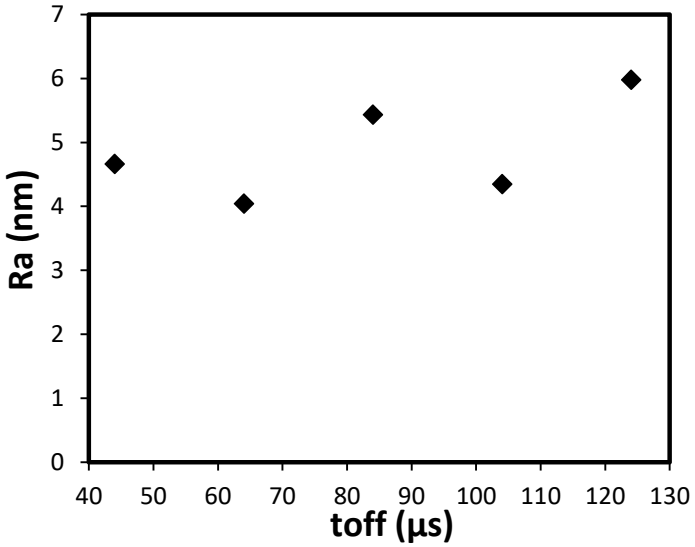

Figure 25: Roughness as function of t_{off} for DLC coatings deposited at 0.8 Pa.

4.2.3 Hardness results as a function of t_{off}

The hardness and Young's modulus of the DLC films deposited by DOMS at different t_{off} and 0.8 Pa working pressure are displayed in Figure 26. The DLC film deposited at a t_{off} of 44 µs has a hardness close to 14 GPa which is the lowest hardness value obtained in this work. Increasing t_{off} to 64 µs results in a significant hardness increase to 19 GPa. This result correlates well the evolution of the change from a clearly columnar to much less columnar microstructure observed in the SEM surface micrographs of the films. Further increasing t_{off} does not significantly change the hardness of the films in agreement with the gradual formation of a featureless microstructure observed by SEM. Note that the maximum hardness, close to 21 GPa, was obtained for the DLC film deposited at t_{off} of 84 µs as was also the case for the films deposited at 0.4 Pa.

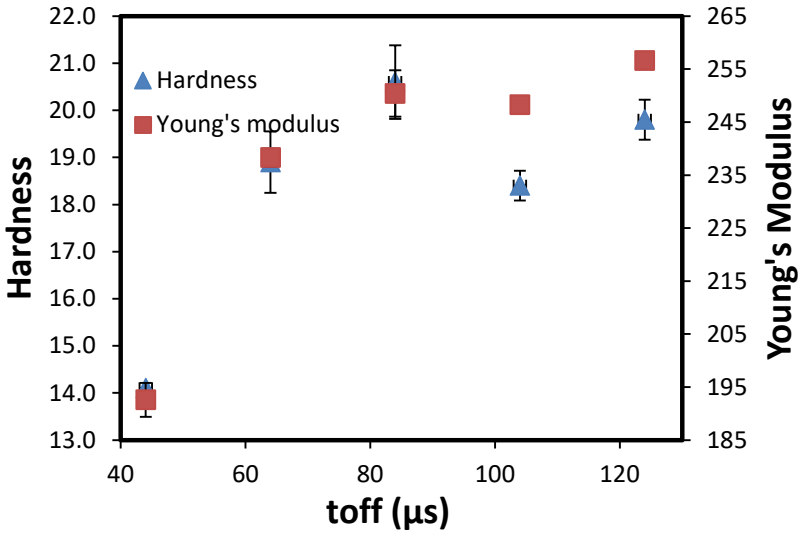

Figure 26: Hardness and Young's modulus of the DLC coatings deposited by DOMS at 0.8 Pa and different values of t_{off}

The maximum depth reached during the nano-indention tests is shown in Figure 27. As mentioned, the opposite trend compared to that of hardness is observed from the graph. Results of maximum depth shows that hardness results are not significantly influenced by substrate as they are only slightly lower than 1/7 of coating thickness.

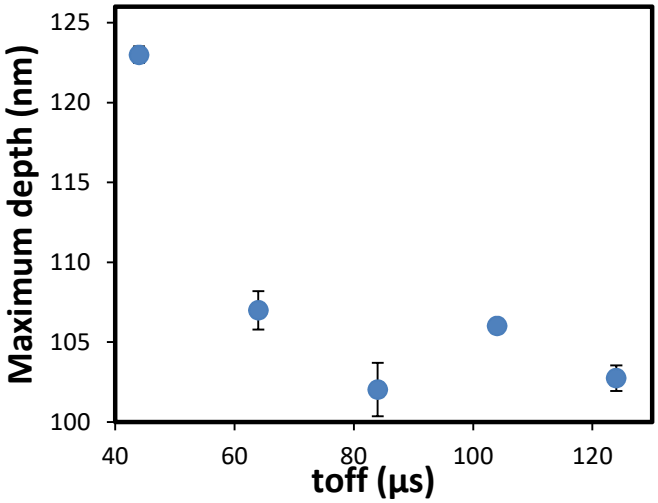

Figure 27: Max depth of the DLC coatings deposited by DOMS at different t_{off}, 0.8 Pa.

4.2.4 Tribological results as a function of t_{off}

The (CoF) versus number of test cycles graph of the DLC coatings deposited at 0.8 Pa, different t_{off} is shown in Figure 28. As for the DLC films deposited at 0.4 Pa, an initial high friction running-in phase is followed by steady state regime where the CoF remains constant.

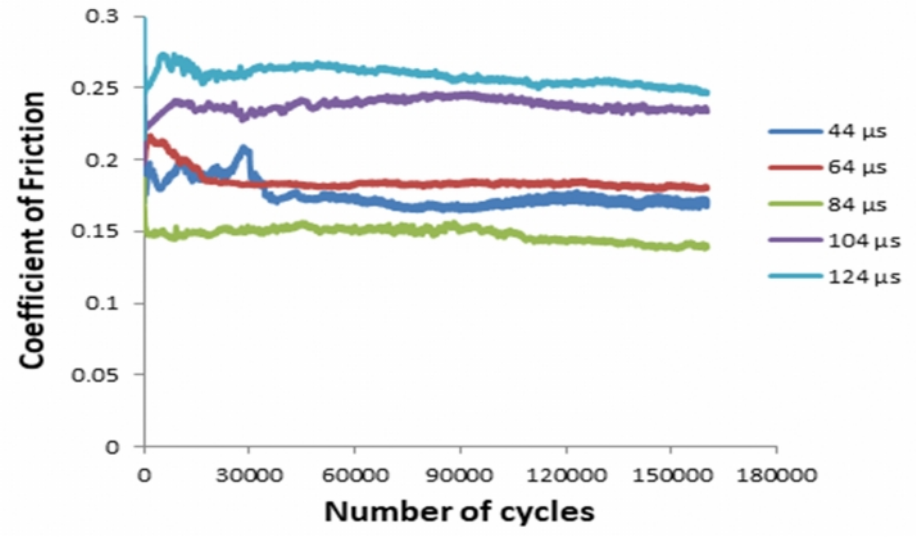

Figure 28: CoF versus number of cycles graph for DLCs deposited at different t_{off}, 0.8 Pa

The average calculated CoF over the steady state region is displayed in Figure 29. The CoF shows a minimum at t_{off} = 84 µs (close to 0.15) while the highest CoF obtained in this work (above 0.24) are found for the films deposited at higher values of t_{off}. The DLC films deposited at 44 and 64 µs have intermediate values for the CoF (0.17 to 0.18).

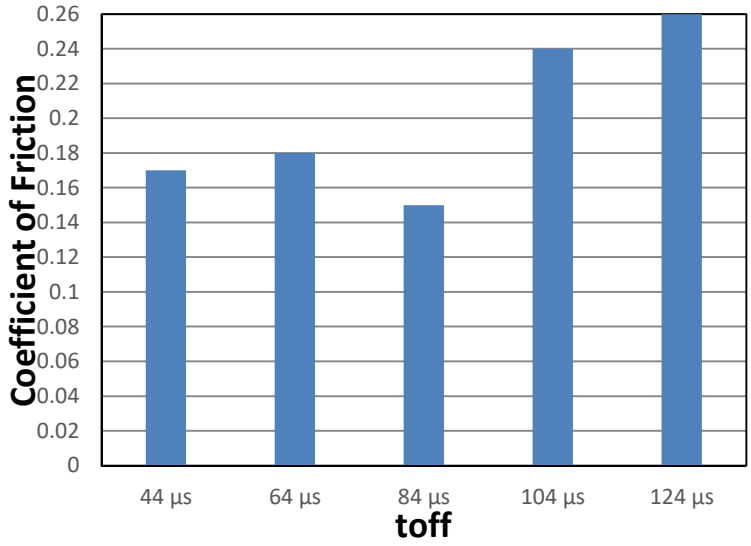

Figure 29: CoF as a function of t_{off} for DLC films deposited at 0.8 Pa

In Figure 30, the specific wear rate of the coatings deposited at different t_{off} is displayed. The specific wear rate of the DLC films initially decreases with increasing t_{off}, increases at intermediate values of t_{off} and finally decreases at the highest value of t_{off}. The lowest value of the specific wear rate measured in this work ($0.22x10^{-16}$ m^3 N^{-1} m^{-1}) was obtained for coating the coating deposited at 64 µs. On the overall, the specific wear rate of the coatings shows large fluctuations that are not obviously correlated either with the DLC films hardness or their friction coefficient.

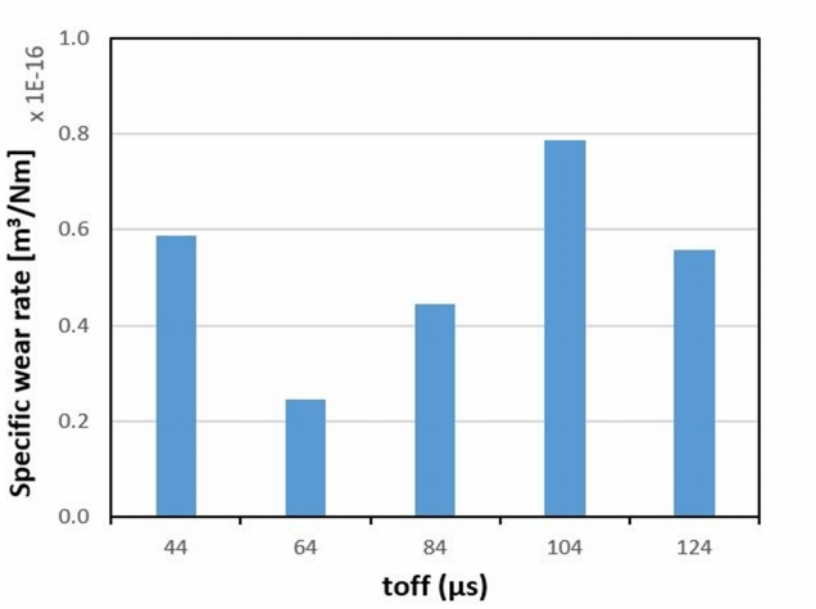

Figure 30: Specific wear rate as a function of t_{off} for DLC films deposited at 0.8 Pa

Figure 31 exhibits the SEM wear tracks and ball wear scar images from optical microscope. As for the coatings deposited at 0.4 Pa, very clean wear tracks can be seen with very little amount of entrained debris and shallow furrows as well. The ball wear scars are also very similar as changing t_{off} in deposition of coating and show a tribofilm which is the significant indication of lower friction coefficients which comply with the results of CoF.

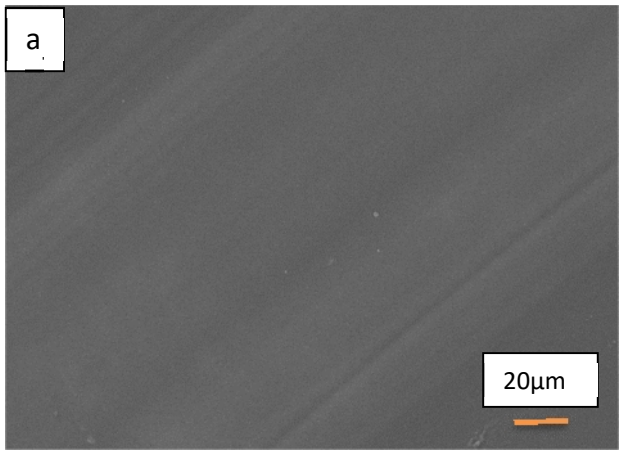
a
20µm

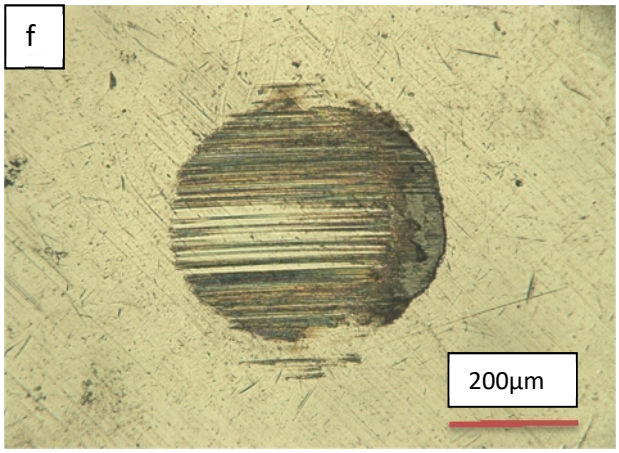
f
200µm

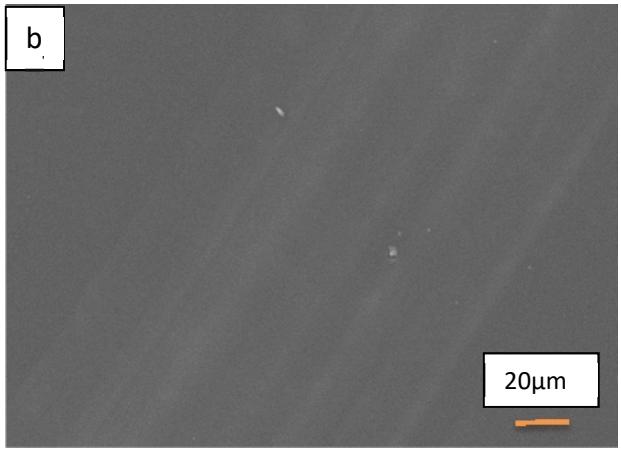
b
20µm

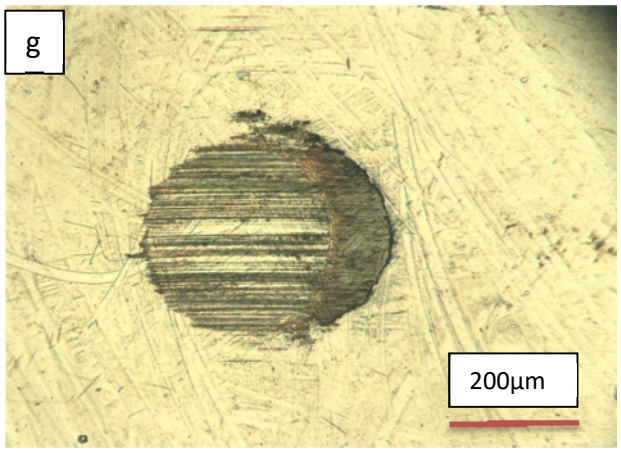
g
200µm

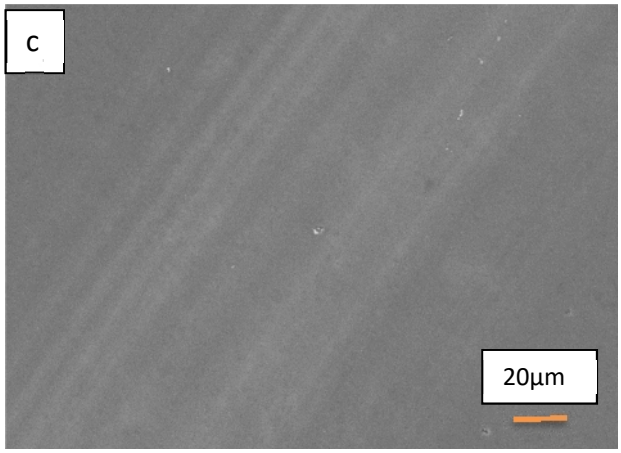
c
20µm

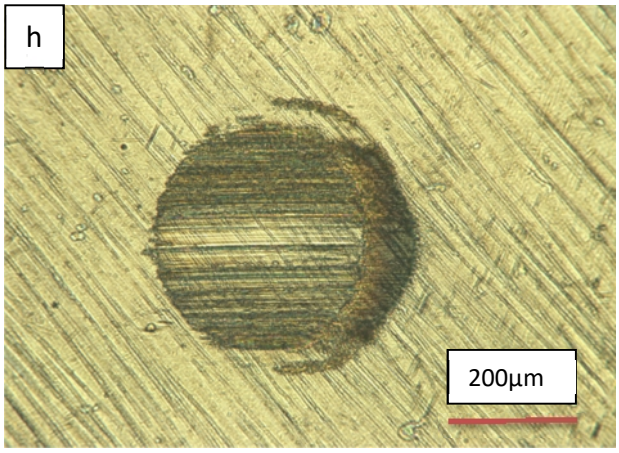
h
200µm

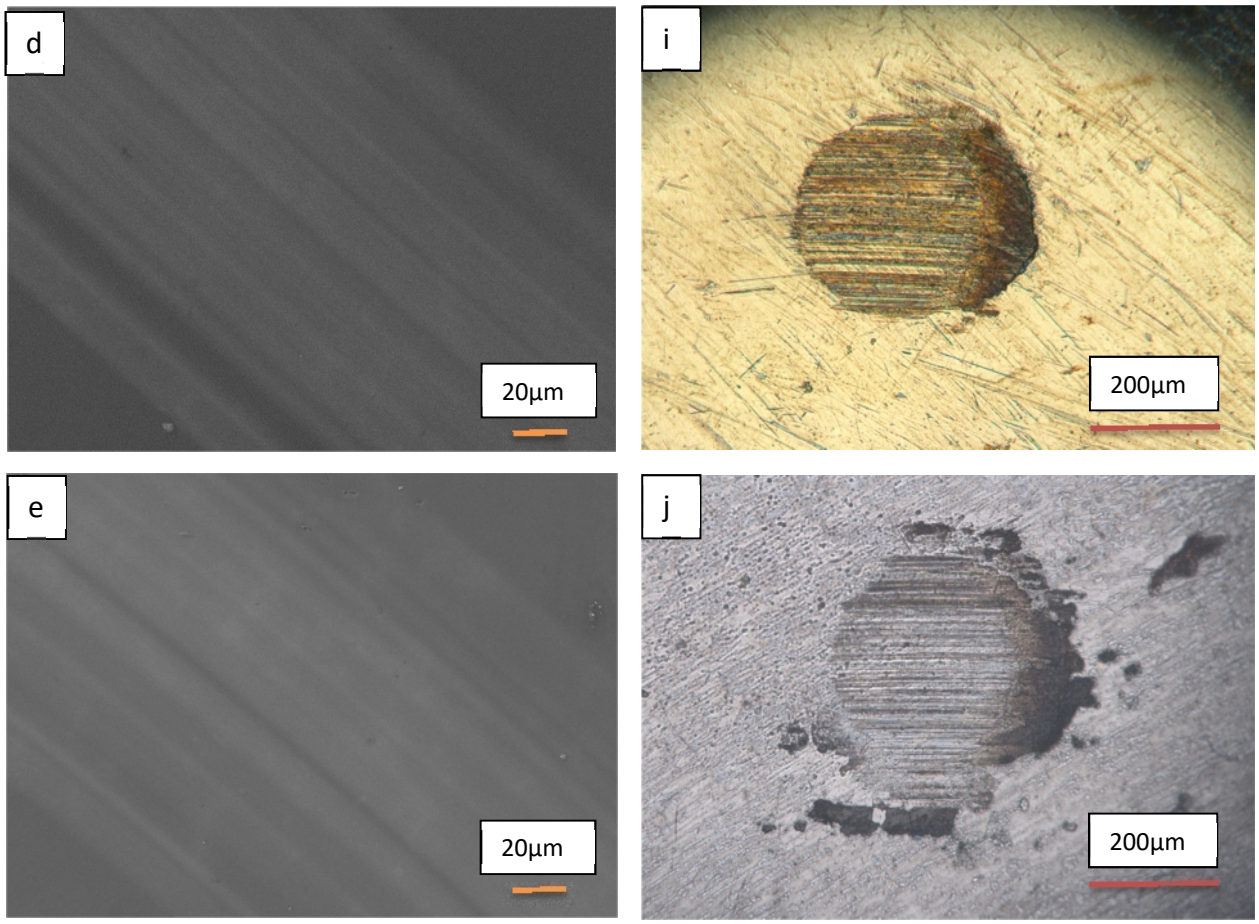

Figure 31: SEM wear track and wear scar images of the DLC coatings deposited by DOMS at 0.8 Pa and t_{off} of a) 44 µs b) 64 µs c) 84 µs d)104 µs; e) 124 µs

4.2.5 Residual stresses as a function of t_{off}

The measured compressive residual stresses of the DLC coatings deposited at 0.8 Pa are shown in Figure 32 as a function of t_{off}. The coating deposited at t_{off} = 64 µs shows the lowest stresses obtained in this work (close to 0.3 Pa). The high stresses in the coating deposited at t_{off} = 64 µs, which are the highest measured in this work, correlate well with the low specific wear rate of the coatings which was the lowest measured in this work. After decreasing to 0.8 GPa stress value at 84 µs, a steady increase is seen and reaches to 1.3 GPa at 124 µs. Once again, on the overall, the compressive residual stresses of all the DLC films are quite low in comparison with the values of several GPa usually referred in the literature for this kind of coatings and should not compromise the performance of the films in service applications.

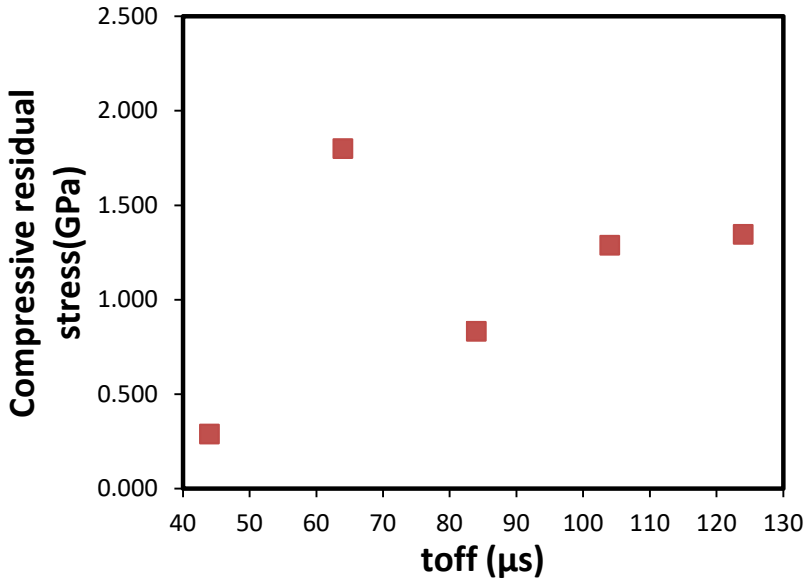

Figure 32: Compressive residual stresses as a function of t_{off} for DLC films deposited at 0.8 Pa

4.3 XPS results

Preliminary XPS measurements were carried out on two of the DLC films deposited in this work. The XPS measurements were carried out on the films deposited at t_{off} = 44 µs, 0.4 and 0.8 Pa. Additionally, two samples deposited in a previous work with substrate bias of – 60 and -80 V at 0.8 Pa were also characterized for comparison purposes. For all samples fast wide range spectra were initially acquired in order to see all elements and their peak positions. Subsequently, detailed spectrum of each peaks (O, C, Ar) were obtained. All the measurements were done without previous ion bombardment of the films surface in order to avoid modifications of their local structure during the cleaning process. The C1s spectrum of carbon of DLC films deposited at different parameters are presented in Figure 33. All the carbon peaks are centred close to 285 although the position of the peaks slightly changes from sample to sample.

In the previous work carried out at CEMMPRE, it was found that bias voltage is the significant parameter which have influence on the sp^3 fraction of DLC films. Thus, the DLC film deposited at -100 V probable shows the highest amount of sp^3 and shifted to the right in the graph. On the other hand, the film deposited at -60 V shows the least amount of sp^3 which is shifted to the left. The coatings from this work (deposited 44 µs, 0.4 Pa and at 44 µs, 0.8 Pa) show the carbon peaks located between the ones of DLCs deposited at -60 V and -100 V as they

are deposited at -80 V. It can be clearly seen that they are located closer to – 60 V which has lower amount of sp^3 fraction. Thus, the first conclusion can be taken that the coatings deposited at short t_{off} has less sp^3 content. The results of XPS are in agreement with the results of hardness as these coating exhibit lower hardness values.

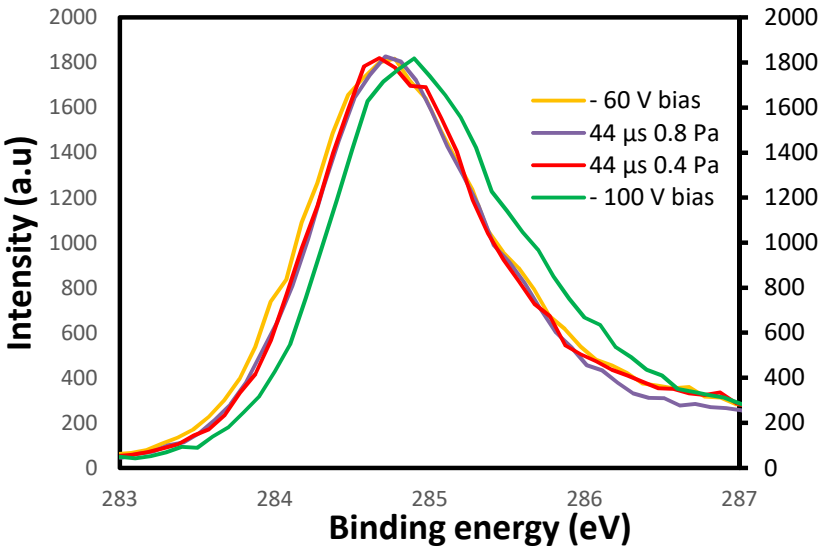

Figure 33: XPS C1s spectrum of DLC films deposited at different parameters.

The main goal of the XPS measurements was to evaluate the sp^3/sp^2 fraction in the films. As the C1s peak position corresponding to sp^2 and sp^3 bonded carbon are slightly different, the sp^3/sp^2 fraction in the films can be estimated from the area of the peaks corresponding to each carbon hybridization state. The curve fitted by Gaussian function is calculated by product of its peak intensity and FWHM. However, the preliminary measurements carried out in this work were not conclusive as it was not possible to fit the C1s carbon peaks, including the DLC films deposited at- 60 and – 100 V, in a consistent manner. Further measurements with higher resolution are necessary in order to evaluate the DLC films sp^3/sp^2 fraction.

Chapter 5: Conclusion and future work

5.1 Conclusion

In this work, DLC films were deposited by DOMS at different oscillation pulse-off time (t_{off}) in two deposition pressures (0.4 and 0.8 Pa). The most significant findings emerging from this study are as follows.

5.1.1 DLC films deposited by DOMS at 0.4 Pa

Regardless of different t_{off} values, all films are smooth and SEM micrographs exhibit similar cauli-flower type morphologies and very dense columnar (almost featureless) microstructure. However the DLC film deposited at the highest t_{off} exhibits a slightly denser microstructure. The hardness is over 15 GPa for all films while the highest hardness is meausured on coating deposited at 84 µs (19.5 GPa). The DLC film deposited at 124 µs shows the lowest CoF (0.11) which is the softest film in this series and in agreement with results of hardness. The lowest specific wear rate (0.43 x 10^{-16} m^3/Nm) was obtained in film deposited at 124 µs. Low residuall stresses are obtained for all films (lower than 1.1 GPa) and peeling-off is not observed. The hardness of the films shows significant changes with t_{off}, most likely due to corresponding changes in the sp^3/sp^2 fraction of the films. However, the specific wear rate of the films remains very similar excepting for the film deposited at the highest t_{off} (124 µs) which has a slightly denser microstructure.

5.1.2 DLC films deposited by DOMS at 0.8 Pa

Although cauli-flower type surface morphologies are observed for all the DLC films, increasing t_{off} results in a much less columnar microstructure which is progressively replaced by featureless microstructure. All the films reveal a hardness close to 20 GPa excepting the one deposited at the lowest t_{off} (44 µs) which displayed the lowest hardness value obtained in this work (14 Gpa). The minimum value of CoF (0.15) is seen on film deposited at 84 µs. The film deposited at 64 µs reveals the lowest specific wear rate obtained in this work (0.25 10^{-16} m^3/Nm).

5.1.3 Final Conclusion

Overall, dramatic differences are not observed in mechanical, tribological and structural properties of DLC films with changing oscillation pulse-off time. This is because the most influent deposition parameter, the substrate bias, was already optimized (-80 V) in the previous work where depositions were carried out at t_{off} values of 124 µs at 0.8 Pa. The main goal of this work was to fine tune the properties of the DLC films by changing t_{off}. All in all, it can be concluded that in first series (0.4 Pa), lowering t_{off} from 124 µs (t_{off} of previous work) doesn't result in improved tribological properties, but better mechanical properties (i.e hardness) is obtained. In the second series (0.8 Pa), decreasing t_{off} from 124 to 84 or even 64 µs results in both a lower friction coefficient and significantly lower wear rates without any appreciable loss of hardness. In fact, the specific wear rate of the film deposited at t_{off} = 64 µs is not only the lowest specific wear rate measures in this work but it is also significantly lower than the specific wear rates measures in previous works about the deposition of DLC films by DOMS.

5.2 Future work

- Further work should be carried out in order to elucidate the relations between the DLC films microstructure, their mechanical properties and their tribological properties. Although some correlations between these properties were found in this work, on the overall it was not possible to found a consistent model that could explain all the obtained results.

- Further XPS analysis should be performed at higher resolution for all the coatings in order to properly evaluate the sp^3/sp^2 fraction in the films and correlate this property with both the mechanical and tribological properties of the films.

- A lubricated tribological study of the DLC coatings at higher temperatures (since working temperature of piston ring is high) and loads should be carried out in the continuation of this project.

References

[1] S. Tung and S. Tseregounis, "An investigation of tribological characteristics of energy conserving engine oils using a reciprocating bench test," *SAE Technical Paper*, 2000.

[2] U. Wallfahrer and L. Bowen, "High performance semisynthetic automotive engine oils using polymer esters as an antiwear booster," *Lubrication engineering*, pp. 23-28, 1998.

[3] A. Morina and A. Neville T. Haque, "Influence of friction modifier and antiwear additives on the tribological performance of a non-hydrogenated DLC coating," *Surface and coating technologies*, vol. 204, pp. 4001-4011, 2010.

[4] J. J. Moore, W. D. Sproul, B. Mishra, Z. Wu and J. Wang J. Lin, "The Structure and Properties of Chromium Nitride Coatings Deposited Using dc, Pulsed dc and Modulated Pulse Power Magnetron Sputtering," *Surface and Coating Technology*, vol. 204, pp. 2230-2239, 2010.

[5] J. Lin and R. Wei, "A comparative study of thick TiSiCN nanocomposite coatings deposited by dcMS and HiPIMS with and without PEMS assistance," *Surface and coating technology*, vol. 338, pp. 84-95, 2018.

[6] C. Donnet and A. Erdemir J. Fontaine, "Fundamentals of the Tribology of DLC Coatings," *Tribology of diamond like carbon films*, pp. 139-154, 2008.

[7] H. Rahnejat, B. Fitzsimons and D. Dowson R. Rahmani, "The effect of cylinder liner operating temperature on frictional loss and engine emissions in piston ring conjunction," *Applied Energy*, pp. 568-581, 2017.

[8] P. Andersson and A. Erdemir K. Holmberg, "Global energy consumption due to friction in passenger cars," *Tribology International*, vol. 47, pp. 221-234, 2012.

[9] R. Jacobs, "Industrial development of carbon-based coatings," in *International Conference on Metallurgical Coatings and Thin Films*, 2017.

[10] H. Cakırer M.B. Karamıs K. Yıldızlı, "An evaluation of surface properties and frictional forces generated from Al–Mo–Ni coating on piston ring," *Applied Surface Science*, 2004.

[11] C.A. Charitidis, "Nanomechanical and nanotribological properties of carbon-based thin films," *Journal of Refractory Metals & Hard Materials*, 2009.

[12] J. Robertson, "Mechanical properties and coordinations of amorphous carbons," *PHYSICAL REVIEW LETTERS*, vol. 68, no. 220, 1992.

[13] D. R. McKenzie, "Tetrahedral bonding in amorphous carbon," *Reports Prog. Phys*, vol. 59, no. 12, pp. 1611-1664, 1999.

[14] J. Robertson, "Diamond-like amorphous carbon," *Materials Science and Engineering*, 2002.

[15] J. Robertson, "Diamond-like amorphous carbon," *Materials Science and Engineering: R: Reports*, vol. 37, no. 4-6, pp. 129-281, 2002.

[16] J.A. Hopwood, "Thin Films: Ionized Physical Vapour Deposition," *Academic Press*, 2000.

[17] C.Donnet and A.Erdemir, "Tribology of Diamond-Like Carbon Films: Fundamentals and Applications," *Springer*, 2008.

[18] Y. Pauleau, "Residual Stresses in DLC Films and Adhesion to Various Substrates in Tribology of Diamond-Like Carbon Films- Fundamentals and applications," *Springer*, pp. 102-138, 2002.

[19] A. Erdemir and C. Donnet, "Tribology of diamond-like carbon films: recent progress and future prospects," *J. Phys. D. Appl*, vol. 39, no. 18, 2006.

[20] C. Rinc'on, G. Zambrano, H. Galindo and P. Prieto N. S'anchez, "Characterization of diamond-like carbon (DLC) thin films prepared by r.f. magnetron sputtering," *Thin solid films*, vol. 373, pp. 247-250, 2000.

[21] C. Davis, M. Weiler, B. Kleinsorge and G. Amaratunga M. Chhowalla, "Stationary carbon cathodic arc: Plasma and film characterization," *Applied physics*, vol. 79, pp. 237-248, 1996.

[22] Y. Yin, G. Amaratunga, D. Mckenzie and T. Frauenhen M. Chhowalla, "Diamond related materials," vol. 6, p. 207, 1997.

[23] D. Callahan, S. McAdams, T. Tsui, S. Anders, A. Anders, J. A. III, I. Brown, C. Bhatia, S. Silva and J. Robertson G. Pharr, "Hardness, elastic modulus, and structure of very hard carbon films produced by cathodic-arc deposition with substrate pulse biasing," *Applied physics letter*, vol. 14, p. 2328, 199.

[24] V.-M. Tiainen and P. Pekko M. Hakovirta, "Techniques for filtering graphite macroparticles in the cathodic vacuum arc deposition of tetrahedral amorphous carbon films," *Diamond related materials*, vol. 8, pp. 1183-1192, 1999.

[25] Peter Siemroth Thomas Witke, "IEEE Trans. Plasma Sci," *1999*, vol. 27.

[26] K. Sridharan and V. Sundaram, "Diamond-like carbon coatings for tribological applications," *Plasma Surface Engineering Research and its Practical Applications*, p. 247, 2008.

[27] J. Robertson, "Deposition mechanism for promoting sp3 bonding in diamond-like carbon," *Diamond Related materials*, vol. 2, pp. 984-989, 1993.

[28] K. Macak, J. Schneider, U. Helmersson and I. Petrov V. Kouznetsov, "A novel pulsed magnetron sputter technique utilizing very high target power densities," *Surface and coating technology*, vol. 122, pp. 290-293, 1993.

[29] A. Braun, C. Zilkens, S. Mráz, J. Schneider, H. Zoubos and P. Patsalas K. Sarakinos, "Exploring the potential of high power impulse magnetron sputtering for growth of diamond-like carbon films," *Surface and coating technology*, vol. 206, pp. 2706-2710, 2012.

[30] K. Sarakinos, D. Lundin, N. Brenning and U. Helmersson A. Aijaz, "A strategy for increased carbon ionization in magnetron sputtering discharges," *Diamond and related materials*, vol. 23, pp. 1-4, 2012.

[31] P. Signumd, *Phys. Rev.*

[32] M. Lattemann, J. Bohlmark, A.P. Ehiasarian, and J.T. Gudmundsson U. Helmersson, "Ionized physical vapor deposition (IPVD): Areview of technology and applications," *Thin Solid Films*, pp. 287-295, 2005.

[33] A. Anders, "Discharge physics of high power impulse magnetronsputtering," *Surf. Coat. Tech.*, no. 205, 2011.

[34] M. Lattemann, J.T. Gudmundsson, A.P. Ehiasarian, Y. Aranda Gonzalvo, N. Brenning, and U. Helmersson J. Bohlmark, "The ion-energy distributions and plasma composition of a

high power impulse magnetron sputtering discharge," *Thin Solid Films*, pp. 1522-1529, 2006.

[35] D. Lundin, J. Jensen, M.A. Raadu, J.T. Gudmundsson, and U. Helmersson M. Samuelsson, "On the film density using high power impulse magnetron sputtering," *Surf. Coat. Tech.*, vol. 15, no. 591, 2010.

[36] J.P. Dauchot, and M. Hecq S. Konstantinidis, "Titanium oxide thin films deposited by high power impulse magnetron sputtering," *Thin Solid Films* , no. 515, p. 1182, 2006.

[37] D. Lundin, P. Larsson, and U. Helmersson A. Aijaz, "Dual- magnetron open field sputtering system for sideways deposition of thin films," *Surf. Coat. Tech*, no. 204, p. 2165, 2010.

[38] C. Christou, A.P. Ehiasarian, U. Helmersson J. Bohlmark J. Alami, *Journal of Vacuum Science & Technology*, 2005.

[39] Mantis deposition ltd. (2015) [Online]. https://www.mantisdeposition.com/mantis/latest-technology/hipims.html.

[40] A. Vetushka and A. P. Ehiasarian, "Plasma dynamic in chromium and titanium HIPIMS discharges," *Journal of Physics D: Applied Physics*, vol. 41, 2007.

[41] Abraham, B. Chistyakov R., "HIPIMS Arc-Free Reactive Sputtering of Non-Conductive Films Using the Endura 200 mm Cluster Tool," 2012.

[42] WilliamD. Sproul, RonghuaWei a, Roman Chistyakov c Jianliang Lin, "Diamond like carbon films deposited by HiPIMS using oscillatory," 2014.

[43] Tao Wang, Jinglin Huang, Zhibing He, Yong Yi, Du. Kai Lei Liu, "Diamond-like carbon thin films with high density and low internal stress deposited by coupling DC/RF magnetron sputtering," *Diam. Relat. Mater*, vol. 70, pp. 151-158, 2016.

[44] R. Kaneko S. Miyake, "Microtribological properties and potential applications of hard, lubricating coatings," *Thin Solid Films*, pp. 256-261, 1992.

[45] J. K.Hirvonen, "Ion beam assisted thin film deposition," *Material science reports*, vol. 6, pp. 215-274, 1991.

[46] S. Varjus, J. Koskinen and K. Holmberg H.Ronkainen, "Differentiating the tribological performance of hydrogenated and hydrogen-free DLC coatings," *Wear*, vol. 249, pp. 260-266, 2011.

[47] Meisam Omidi Atena Fatehinya Masomeh Farahani Zahra Akbari Saleheh Shahmorad Fatemeh Yazdian Mohammadreza Tahriri Keyvan Moharamzadeh Lobat Tayebi Daryoosh Vashaee, "Characterization of biomaterials," *Biomaterials for Oral and Dental Tissue Engineering*, pp. 97-115, 2017.

[48] S. Wischnitzer, *Introduction to Electron Microscopy*. New York: Pergamon Press, 1962.

[49] K.S. Howard, A.H. Johnson and K.L. McMichael M.T. Postek, *Scanning Electron Microscopy*. Inc. Williston: Ladd Research Ind, 1980.

[50] P. Rhodri Williams Matthew S. Barrow, "Atomic Force Microscopy in Process Engineering," 2009.

[51] M. Roy, "Protective Hard Coatings for Tribological Applications," *Materials Under Extreme Conditions*, 2017.

[52] R.R.Mather, "Surface modification of textiles by plasma treatments," *Woodhead Publishing Series in Textiles*, pp. 296-317, 2009.

[53] Andrew Fogden Per M. Claesson, *Handbook for Cleaning/Decontamination of Surfaces*., 2007.

[54] Donald M. Mattox, *Handbook of Physical Vapor Deposition (PVD) Processing (Second Edition)*., 2010.

[55] Laurence W.McKeen, "Introduction to the Tribology of Plastics and Elastomers," in *Fatigue and Tribological Properties of Plastics and Elastomers (Second Edition)*., pp. 25-38.

[56] Curtis D. Johnson, *Displacement, Location, or Position Sensors, Process Control Instrumentation Technology*.: Prentice Hall PTR, 1997.

[57] R. Serra, A. Cavaleiro, J. Oliveira F. Ferreira, "Additional control of bombardment by deep oscillation magnetron sputtering:effect on the microstructure and topography Cr thin films," *Thin Solid Films*, no. 619, pp. 250-260, 2016.

[58] S. Kasi, J. Rabalais, W. Eckstein Y. Lifshitz, "Subplantation model for film growth from hyperthermal species," *Phys. Rev*, no. 10468, 1990.

[59] Asim Aijaz, Tomas Kubart, Albano Cavaleiroa, João Oliveiraa Fábio Ferreira, "Hard and dense diamond like carbon coatings deposited by deep oscillations," *Surface& Coatings technology*, 2017.

[60] D. Muller, B. Pailthorpe D. McKenzie, "Compressive-stress-induced formation of thin-film tetrahedral amorphous carbon," *Phys. Rev. Lett*, no. 773, 1991.

[61] Helena Ronkainen, "Tribological properties of hydrogenated and hydrogen free DLC coatings," Technical research centre of Finland, Finland, 2001.

[62] Erdemir A, Meletis EI Liu Y, "DLC coatings for mechanical applications," *Surf Coat Technol*, vol. 82, 1996.

[63] et al A.C. Ferrari, *Diam. Relat. Mater*, pp. 994-999, 2002.